Article

The small GTPase MRAS is a broken switch

Gabriela Bernal Astrain[1,2], Regina Strakhova[1,2], Chang Hwa Jo [1],
Emma Teszner[1,2], Ryan C. Killoran[1] & Matthew J. Smith [1,2,3] ✉

Intense research on founding members of the RAS superfamily has defined our understanding of these critical signalling proteins, leading to the premise that small GTPases function as molecular switches dependent on differential nucleotide loading. The closest homologs of H/K/NRAS are the three-member RRAS family, and interest in the MRAS GTPase as a regulator of MAPK activity has recently intensified. We show here that MRAS does not function as a classical switch and is unable to exchange GDP-to-GTP in solution or when tethered to a lipid bilayer. The exchange defect is unaffected by inclusion of the GEF SOS1 and is conserved in a distal ortholog from nematodes. Synthetic activating mutations widely used to study the function of MRAS in a presumed GTP-loaded state do not increase exchange, but instead drive effector binding due to sampling of an activated conformation in the GDP-loaded state. This includes nucleation of the SHOC2-PP1Cα holophosphatase complex. Acquisition of NMR spectra from isotopically labeled MRAS in live cells validated the GTPase remains fully GDP-loaded, even a supposed activated mutant. These data show that RAS GTPases, including those most similar to KRAS, have disparate biochemical activities and challenge current dogma on MRAS, suggesting previous data may need reinterpretation.

Principal gatekeepers of signal transduction are small GTPase proteins, which typically function as 'molecular switches' by exchanging between two structural conformations. In the active, GTP-bound state they bind effector proteins that initiate signaling cascades directing growth, differentiation, survival, and motility. A conformational change elicited by GDP in the active site prevents effector binding. Three GTPase homologs are fundamental regulators of normal development and drivers of human cancers. Point mutations lock HRAS, KRAS and NRAS (hereon H/K/NRAS or classical RAS) in an activated state, driving constitutive proliferation[1]. Their impact on human health has made H/K/NRAS foremost targets of cancer therapeutics and a major research focus for four decades, meaning this subset of proteins has come to define our understanding of small GTPase function. Cancer-causing point mutations locking H/K/NRAS in a GTP-bound state have been widely used to enable study of the large ~160 member RAS superfamily, which includes GTPases of the RAS, RHO, ARF, RAB and RAN subgroups[2]. This is despite a notable lack of biochemical data exploring the function of most family members, though the nucleotide

switch is believed a fundamental property of these signaling enzymes. The few exceptions include atypical RHO GTPases (RND class[3] and RHOH[4]) that bind GTP but have no enzymatic activity, and RHOBTB proteins that do not bind nucleotides[5,6]. These proteins are now classified as pseudoGTPases[7]. RGK proteins of the RAS subfamily (REM1, REM2, GEM and RRAD) may constitute another class, as they do not undergo conformational change with nucleotide cycling[8,9], and some ARF GTPases do not bind nucleotides or have significantly higher affinity for GTP[10].

The early discovery of three related GTPases (RRAS, RRAS2 and MRAS) with the highest homology to H/K/NRAS was met with a large effort to elucidate their effectors and signaling activity. Point mutations at the G12 and Q61 hotspots were introduced to RRAS GTPases expressed in cells, while their in vitro activity was studied using artificial loading of non-hydrolyzable nucleotides (GTPγS or GMPPNP). Such approaches determined that RRAS GTPases utilize a similar array of effectors as H/K/NRAS and trigger cellular transformation via the MAPK pathway, yet these proteins are rarely mutated in human

[1]Institute for Research in Immunology and Cancer (IRIC), Université de Montréal, Montréal, QC H3T 1J4, Canada. [2]Programmes de biologie moléculaire, Université de Montréal, Montreal, QC H3C 3J7, Canada. [3]Department of Pathology and Cell Biology, Faculty of Medicine, Université de Montréal, Montréal, QC H3T 1J4, Canada. ✉e-mail: matthew.james.smith@umontreal.ca

cancers. How such close homologs are unable to drive tumourigenesis remains an open but vital question. Interest in MRAS was invigorated by the discovery that an MRAS[Q71L] mutant binds a unique effector called SHOC2 and the phosphatase PP1Cα to regulate RAS-induced proliferation[11,12]. This holophosphatase complex is anchored by the leucine rich repeats (LRR) of SHOC2 and is proposed to dephosphorylate RAF kinases to permit full induction of the MAPK cascade. The SHOC2-MRAS-PP1 (SMP) complex may explain why MRAS is overexpressed in some human cancers[13–16] and why *MRAS* mutations are present in RASopathies[17–20], developmental disorders driven by subtle activation of MAPK signaling. This has made MRAS a clinical target of enormous interest, culminating with four recent papers[21–24] describing the SMP structure. Each revealed MRAS nucleates complex formation in a nucleotide-dependent manner (i.e. only when GMPPNP(GTP)-loaded), but also that H/K/NRAS can functionally replace MRAS at slightly reduced affinities.

We show here that wild-type MRAS, despite high homology to H/K/NRAS, is a pseudoGTPase switch deficient in GTP loading and this property is conserved in distal MRAS orthologs. Hotspot mutants derived from H/K/NRAS oncoproteins remain GDP loaded but adopt an activated conformation capable of effector binding. This has important implications for the study of small GTPases using RAS-derived point mutations and should ultimately provide avenues to inhibit H/K/NRAS activation.

Results

MRAS does not exchange GDP-to-GTP and is insensitive to GEF

With growing interest in the RRAS subfamily of GTPases, particularly MRAS, we reconsidered the nucleotide cycling kinetics of these proteins. This has been poorly investigated since their initial discovery, but even minor differences in activity could explain why *RRAS* and

RRAS2 mutations are rare in cancer[25–27] and *MRAS* is not mutated. To investigate this, we used a real-time nuclear magnetic resonance (RT-NMR) spectroscopy approach that offers a significant advantage over the most frequently used assays of GTPase activity: observation and quantitation of nucleotide cycling is based on direct visualization of protein conformation, rather than indirect measurements of bound versus free nucleotide. To begin, we purified recombinant human RRAS, RRAS2 and MRAS from *E. coli* with uniform ^{15}N-labeling. These proteins lacked the C-terminal hypervariable region (HVR) to increase their expression and stability (referred to hereon as ΔC), as is typical of in vitro experiments with RAS GTPases. All three GTPases purified from bacteria were GDP-bound. To first characterize spectral changes induced by differential nucleotide loading, RRAS proteins loaded with GDP or forced-exchanged with GMPPNP (non-hyrolyzable GTP analog resistant to phosphatase activity) had benchmark spectra acquired by NMR. To study nucleotide exchange, GDP-loaded proteins were incubated with a tenfold molar excess of GTPγS (non-hydrolyzable GTP analog; consistent with the GTP:GDP ratio found in cells[28]), and for hydrolysis the proteins were loaded with GTP. RT-NMR analyses of nucleotide cycling was performed with BEST-HSQCs and assays with RRAS and RRAS2 (Fig. 1a) revealed the proteins hydrolyze GTP at the same rate as HRAS[29] and exchange GDP-to-GTP at slightly increased rates (2.2-fold and 2.4-fold, respectively). In contrast, though we could force-load MRAS with GMPPNP (Fig. 1b) this GTPase was unable to undergo intrinsic nucleotide exchange. Even incubation with a 20-fold molar excess of GTPγS and addition of the catalytic subunit (SOS[cat]) from its alleged GEF, SOS1[30], did not stimulate MRAS exchange (Fig. 1c). These data suggested a fundamental difference in MRAS activity that had not been previously observed.

To elucidate mechanisms behind the MRAS defect we considered possible biochemical pretexts. First, as initial assays were done with
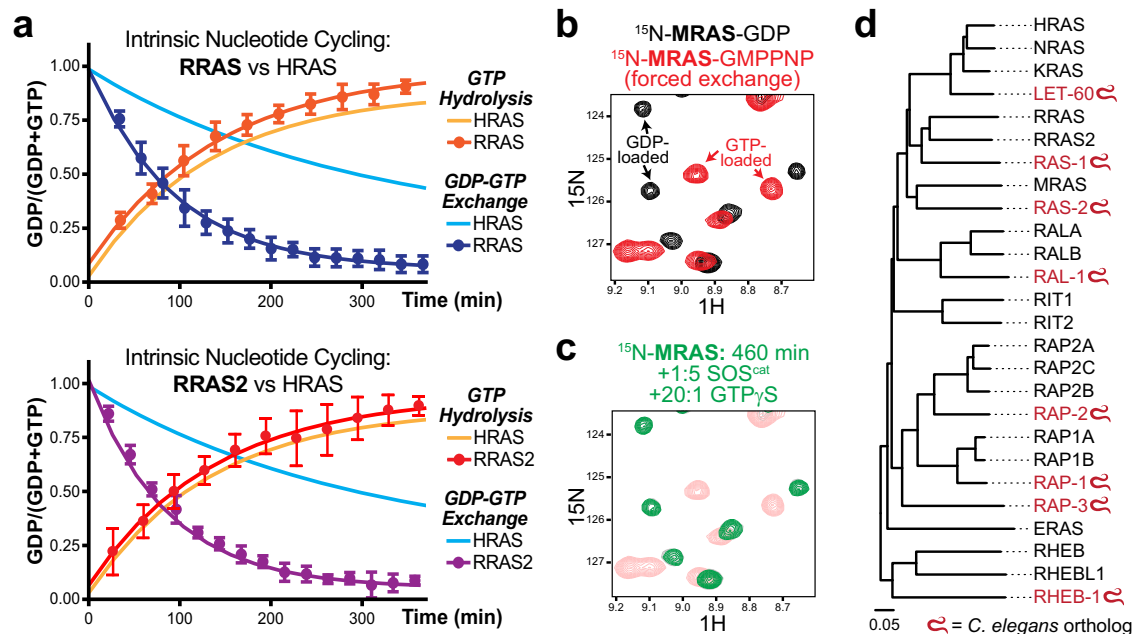

Fig. 1 | MRAS does not intrinsically exchange GDP for GTPγS in vitro. a Intrinsic nucleotide exchange and hydrolysis curves for HRAS (K_{exch}=3.4 ± 0.1 × 10^{−3} (light blue) and K_{hydro} = 7.5 ± 0.1 × 10^{−3} (yellow)), RRAS (top panel, K_{exch} = 10.7 ± 0.3 × 10^{−3} (dark blue) and K_{hydro} = 6.8 ± 0.2 × 10^{−3} (orange)), and RRAS2 (bottom panel, K_{exch} = 8.2 ± 0.7 × 10^{−3} (purple) and K_{hydro} = 7.4 ± 0.3 × 10^{−3} (red)). Curves were obtained using changes across multiple peak intensities extracted from sequential ^{1}H/^{15}N HSQC spectra of isotopically labeled GTPases. Plotted are mean ± standard deviation. *n* = 3 experiments were performed independently with similar results. GTPases were incubated in a tenfold molar excess of GTPγS to measure exchange.

For hydrolysis, GTPases were preloaded with GTP and incubated in the magnet at 25 °C. **b** NMR spectra show distinct chemical shifts specific to GDP or GMPPNP-bound MRAS. Overlay is of ^{1}H/^{15}N HSQC spectra from force-loaded MRAS-GDP (black) and MRAS-GMPPNP (red). **c** MRAS shows no change in nucleotide binding after the addition of 20:1 excess GTPγS and 1:5 molar ratio of the catalytic subunit from its alleged GEF, SOS1 (SOS[cat]). Green spectrum is from ^{15}N-MRAS incubated with GTPγS/SOS[cat] for 460 min. **d** Phylogenetic tree of human RAS GTPase subfamilies with orthologs from *C. elegans* (red). Source data are provided as a Source Data file.

MRASΔC we purified full length MRAS (1-205), missing only 3 C-terminal residues of the CaaX motif typically removed during post-translational processing in cells. This protein was stable in solution and purified in a GDP-bound state but did not undergo GDP-to-GTP exchange (Supplementary Fig. 1a). We next considered whether tethering to a membrane might drive MRAS activation as it possesses a prenylation motif and polybasic region in its HVR. Previous work using small lipid bilayer nanodiscs[31] has shown that membrane tethering can affect nucleotide exchange of some GTPases[32]. We assembled nanodiscs using the membrane scaffold protein MSP1D1 and tethered MRAS by its C-terminal Cys205 residue (Supplementary Fig. 1b). To permit analysis by NMR, MRAS was selectively labeled with ^{13}C-Ileδ1. GDP-bound or protein force-loaded with GMPPNP confirmed that ^{1}H-^{13}C HSQCs could differentiate between the two nucleotide-bound states. Unlike KRAS[33], when MRAS was loaded with GMPPNP the presumed Ile31 peak (analogous to KRAS-Ile21 and at the same chemical shift) was not perturbed but rather broadened beyond detection, meaning only loss of this resonance reports on MRAS nucleotide loading. This could be resolved when force exchanged proteins were tethered to nanodiscs (Supplementary Fig. 1c), however, when MRAS-GDP nanodisc assemblies were incubated with 10:1 GTPγS for 12 h there was no observable nucleotide exchange, implying a more fundamental defect in MRAS activity.

A lack of exchange activity in distal orthologs of MRAS would reveal functional conservation. The nematode *C. elegans* has a complete set of RAS orthologs, including LET-60 (KRAS), RAS-1 (RRAS/2) and RAS-2 (MRAS) (Fig. 1d). We purified isotopically labeled LET-60 and RAS-2 and performed exchange assays by RT-NMR. This confirmed that LET-60 is a functional GTPase switch able to exchange GDP-to-GTP, but RAS-2 was completely deficient (Supplementary Fig. 1d, e). This validates lack of GTP binding as an inherent biochemical trait of MRAS. Importantly, small GTPases are not actively loaded with GTP but rather bind this nucleotide upon GDP release because it is tenfold more abundant in cells. H/K/NRAS have similar affinities to these nucleotides, but lack of MRAS exchange suggests a higher affinity for GDP. To verify this and establish our purified MRAS as functional we performed a reverse exchange: force-loaded MRAS-GMPPNP was incubated with GDP and exchange monitored by RT-NMR (Supplementary Fig. 2a). In these conditions, MRAS rapidly exchanged GMPPNP-to-GDP, confirming increased affinity for GDP. Finally, we questioned whether MRAS may retain GTPase activity despite poor affinity for this nucleotide. Unlike H/K/NRAS or the RRAS/2 proteins, loading of MRAS with GTP was extremely challenging. To accomplish this required force-loading of MRAS with GMPPNP (allowing use of phosphatase to remove all GDP) followed by attempted loading with GTP. This resulted in a substantial GTP-loaded fraction of MRAS (~50%), allowing monitoring of hydrolysis activity by RT-NMR. This revealed MRAS does indeed retain activity (Supplementary Fig. 2b). Taken together, while MRAS has a potential GTPase function its high affinity for GDP and complete lack of nucleotide exchange suggest the protein must normally function in a GDP-bound state.

MRAS synthetic mutants remain GDP-loaded yet bind effectors

MRAS was shown to bind similar effectors to H/K/NRAS, and more recently to form a holophosphatase complex with SHOC2-PP1Cα. Evidence for these complexes has relied on synthetic activation of MRAS in cells based on RAS oncomutants, or on GMPPNP-loading in vitro. Our data indicate wild-type MRAS cannot be GTP-loaded and we sought to reconcile this with previous results. Though we did not observe activation of the MAPK pathway following expression of MRAS^{G22V} in cultured cells (analogous to RAS^{G12V}; Supplementary Fig. 2c), this synthetic mutant could be specifically precipitated from cell lysates by the BRAF-RAS-binding domain (RBD), while wild-type MRAS was not (Supplementary Fig. 2d). Isothermal titration calorimetry (ITC) revealed that MRAS^{WT} exchanged with GMPPNP could bind

directly to the BRAF-RBD, a canonical H/K/NRAS effector, with an affinity of 8.3 μM (Supplementary Fig. 2e). This was dependent on GMPPNP loading as no binding was detected to MRAS^{WT}-GDP. This affinity is 62-fold weaker than BRAF-RBD binding to KRAS^{WT}-GMPPNP (0.13 μM), yet evidence of direct, nucleotide-dependent binding together with the precipitation of synthetic mutants from cells suggested the widely-used mutants of MRAS may undergo exchange. To test this, we purified isotopically labeled MRAS^{G22V} and MRAS^{Q71L} (based on RAS^{Q61L}) and monitored GDP-to-GTPγS exchange by RT-NMR (Fig. 2a). Like the wild-type protein, these MRAS mutants remained fully GDP loaded. We also assayed a G23V mutant of MRAS previously identified in a patient with Noonan Syndrome and believed causative of this developmental disorder[17]. As with wild-type MRAS and the synthetic mutants, this variant was completely defective in GDP-to-GTP exchange (Supplementary Fig. 2f). Previous work has shown that addition of cell lysate can directly stimulate small GTPase cycling when monitored by RT-NMR[29,34]. To determine if cellular factors in whole lysates could activate MRAS^{Q71L}, we added 40 μl of concentrated HEK 293T lysate and 10:1 GTPγS but there was still no evident exchange (Supplementary Fig. 2g). These results suggest a distinct activation mechanism imparted by synthetic mutation of MRAS that is not GTP-dependent.

To elucidate how MRAS G22V/Q71L mutants confer an ability to bind the BRAF-RBD we considered whether these variants may adopt an activated conformation while GDP bound. Indeed, previous study of the KRAS^{G12V} oncoprotein suggest it samples an active-like conformation when loaded with GDP[35]. To test this, we first conducted in vitro binding assays using purified GST-BRAF-RBD with KRAS or MRAS variants. Binding of both wild-type KRAS and MRAS to the RBD was completely dependent on GMPPNP-loading (Fig. 2b). In contrast, synthetic mutants of MRAS were also precipitated by the RBD in a GDP-bound state, though to a lesser extent than GMPPNP-loaded proteins (Fig. 2c). To further observe whether MRAS-GDP samples multiple conformational states we turned to ^{31}P-NMR. By monitoring chemical shifts of nucleotide phosphates this approach previously revealed a conformational equilibrium of H/K/NRAS in two distinct states when GTP/GMPPNP loaded (state 1=inactive and state 2=active)[36–38]. We acquired ^{31}P spectra of 1 mM MRASΔC following GMPPNP loading and observed it also adopts two conformational states, though primarily exists in state 1 compared to KRASΔC (Supplementary Fig. 3a). Initial experiments with full-length, GDP-loaded MRAS variants (wild-type, G22V and Q71L) showed no evidence of a second conformation (Supplementary Fig. 3b). However, MRAS^{G22V}ΔC lacking the HVR had a clear secondary conformation detected by the α-phosphate resonance that was not present in wild-type spectra (Fig. 2d). Upon addition of fivefold molar excess (5 mM) BRAF-RBD to full-length MRAS^{G22V}-GDP a peak could be detected in the same region, indicating that RBD binding to MRAS^{G22V} stabilizes the state 2 conformation. This additional resonance was not evident when the RBD was added to MRAS^{WT} or MRAS^{Q71L}. To further corroborate the hypothesis that GDP-loaded MRAS mutants can bind RBD we used ^{1}H-^{13}C SOFAST-HMQC detection of ^{13}C-Ileδ1 labeled MRAS. When wild-type or G22V/Q71L mutants of MRAS were force loaded with GMPPNP, a unique chemical shift could be detected upon mixing with a twofold molar excess of unlabeled BRAF-RBD (Fig. 3a). Experiments with GDP-loaded proteins revealed all 13 Ile of MRAS are evident, and that wild-type has no further resonances (Fig. 3b). In contrast, MRAS^{G22V} has an additional chemical shift adjacent to the presumed Ile31 peak, suggesting this resonance is split when MRAS^{G22V} is GDP-bound and the corresponding region (switch 1) samples two conformations. Intensity of this secondary peak was increased at 37 °C. An additional peak was also visible for MRAS^{Q71L}, but to a lesser extent and the spectrum more resembled wild-type. When unlabeled RBD was added to these GDP-loaded proteins it had no effect on wild-type MRAS and all 13 Ile chemical shifts were unchanged (Fig. 3c). However, the RBD induced several chemical shift
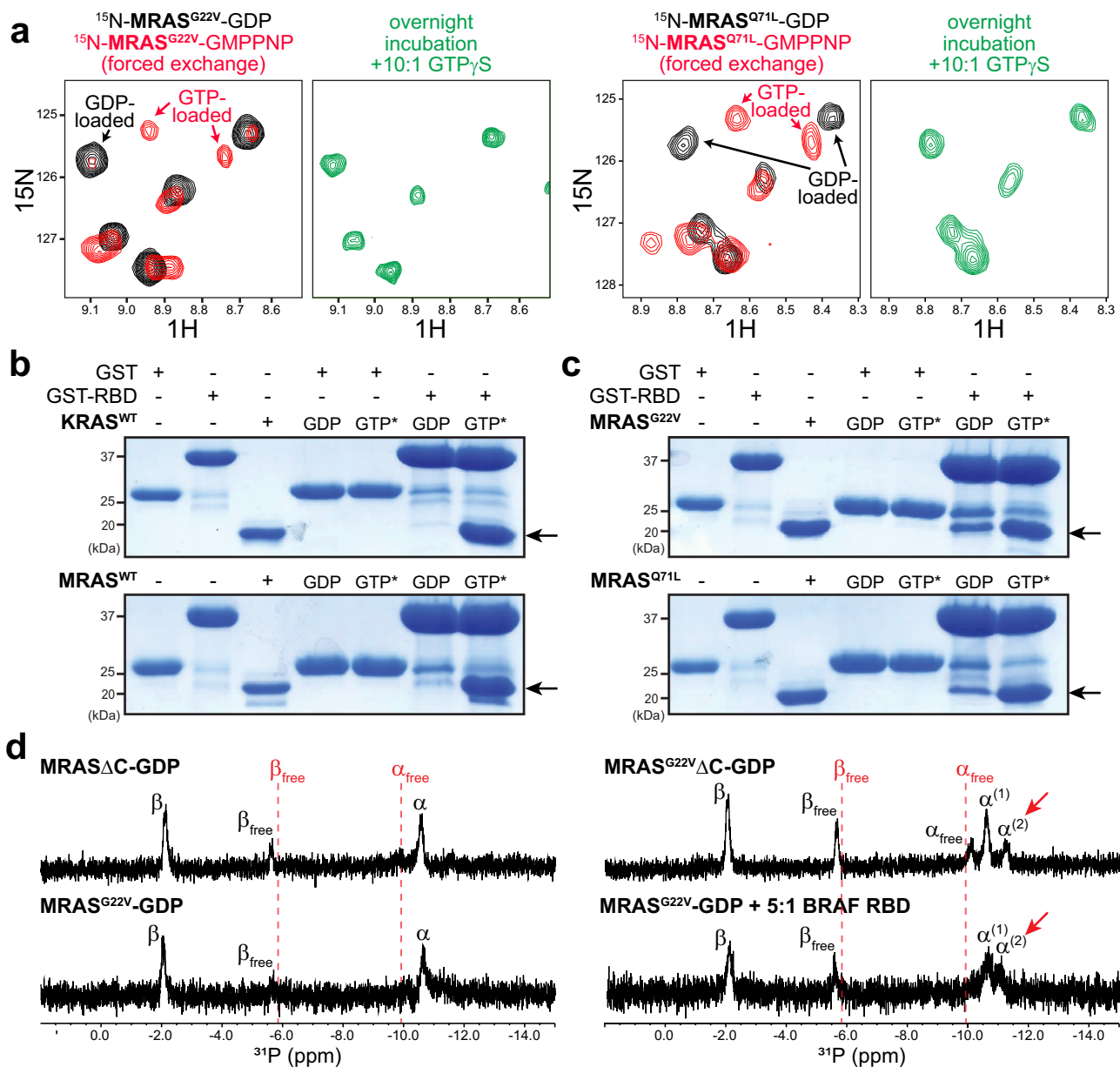
Fig. 2 | Mutationally 'activated' MRAS is also defective in GDP-to-GTPγS exchange yet binds the RAF RBD when GDP-loaded. a Mutants used to study MRAS in a constitutively active state show no intrinsic exchange. Overlays of ^{1}H/^{15}N HSQC spectra of MRAS^{G22V} (left) and MRAS^{Q71L} (right) bound to GDP (black) or GMPPNP (red) show resonances specific to each nucleotide-bound state. HSQC spectra after overnight incubation with 10:1 molar excess GTPγS are in green. **b** Interaction between the BRAF RBD and both KRAS^{WT} (top) and MRAS^{WT} (bottom) is nucleotide dependent. In vitro binding assays mixed 2 μM recombinantly purified, GST-BRAF-RBD or GST alone control with 25 μM purified RAS GTPases. Complexes were precipitated on glutathione beads followed by washing to remove non-specific binders. Arrows indicate where precipitated GTPases should appear. KRAS and MRAS were pre-loaded with the nucleotides indicated at top (GTP* refers to the analog GMPPNP). n = 3 experiments were performed independently with similar results. **c** MRAS^{G22V} (top) and MRAS^{Q71L} (bottom) bind the BRAF RBD when either GTP* or GDP-loaded. MRAS mutants were pre-loaded with the nucleotides indicated at top (GTP* refers to GMPPNP). n = 3 experiments were performed independently with similar results. **d** 1D ^{31}P-NMR spectra reveal MRAS^{G22V} samples two conformations when GDP bound. Spectra include GDP-loaded MRAS^{WT}ΔC, MRAS^{G22V}ΔC, MRAS^{G22V} and MRAS^{G22V} incubated with a 5:1 molar excess BRAF RBD. α and β labels represent the α- and β-phosphate resonances. (1) and (2) represent state 1 and state 2 conformations of the GTPase, and 'free' is unbound nucleotide. Spectra were recorded using 1 mM purified proteins. Source data are provided as a Source Data file.

perturbations in MRAS^{G22V} and MRAS^{Q71L} that validated these variants could bind BRAF-RBD independent of nucleotide. These data reveal that MRAS synthetic mutants adopt an activated conformation in the GDP-bound state and suggest their use drives binding to effectors.

MRAS activation is proposed to nucleate formation of the SHOC2-MRAS-PP1Cα (SMP) complex, initially discovered using MRAS^{Q71L}. All four SMP complex structures were derived with MRAS-GMPPNP, which can be generated in vitro using phosphatase-

mediated degradation of GDP. As our data indicated MRAS^{Q71L} may adopt an activated conformation despite being GDP loaded, we examined whether this variant could nucleate the SMP complex when GDP-bound. We first verified previous results showing MRAS^{WT} only binds SHOC2-PP1Cα when GMPPNP-loaded. Purified SHOC2 and PP1Cα were mixed with MRAS and complexes elucidated by gel filtration (Fig. 4a). Indeed, MRAS^{WT}-GDP could not form the holoenzyme. In contrast, the same experiment with MRAS^{Q71L} showed the
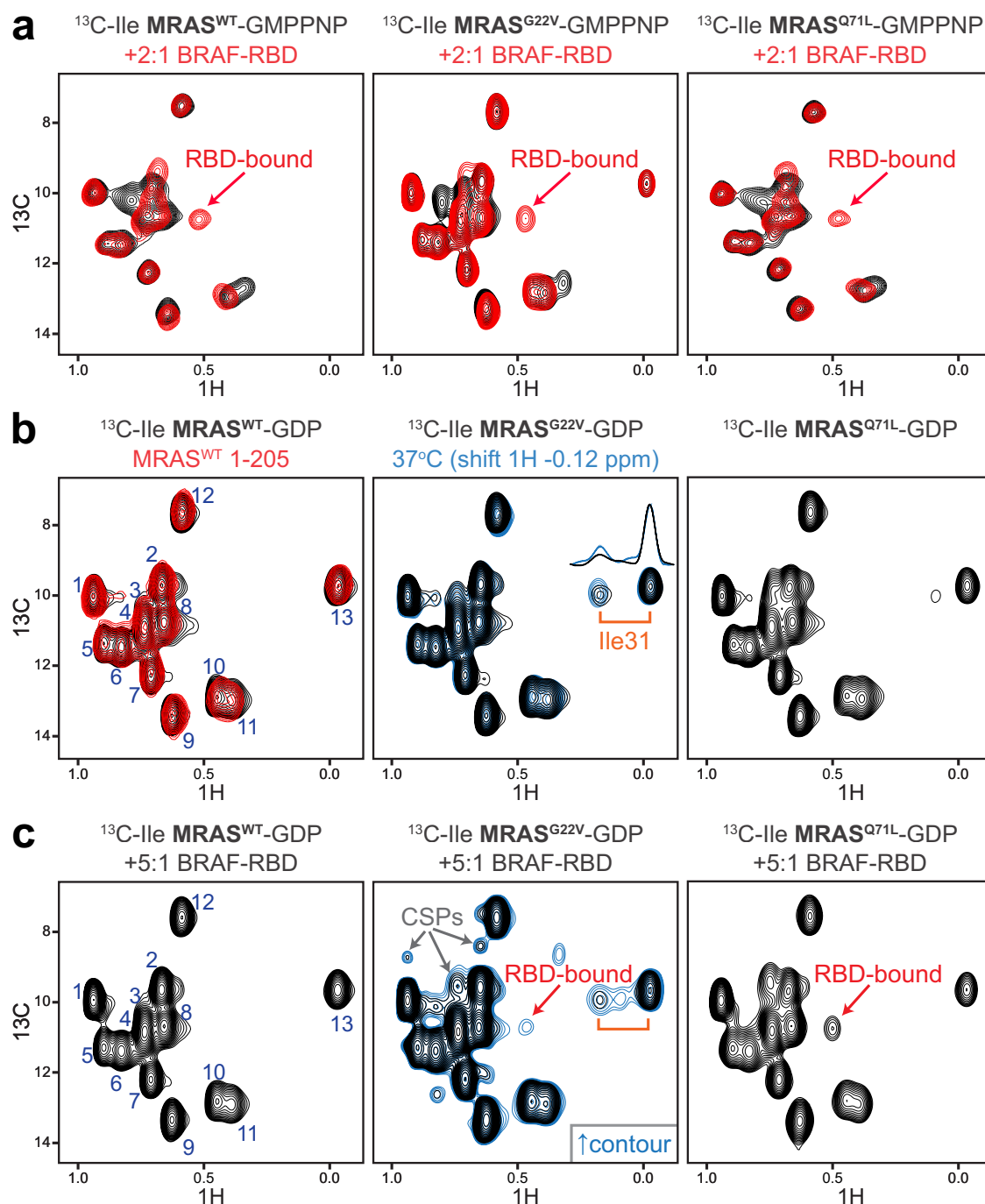
Fig. 3 | MRAS^{G22V} and MRAS^{Q71L} adopt an RBD-binding conformation when GDP bound. a The RBD of BRAF binds MRAS variants force loaded with GMPPNP. ^{13}C-Ileδ1 MRAS wild-type (left), G22V (middle) or Q71L (right) were incubated in a twofold molar excess of unlabeled RBD domain. SOFAST-HMQCs revealed a consistent chemical shift reporting on the bound state for each variant (middle of red spectra, marked with arrows). **b** SOFAST-HMQCs of wild-type (left), G22V (middle) and Q71L (right) ^{13}C-Ileδ1 MRAS bound to GDP. All 13 Ile are detected for both full length (1-205) and ΔC (1-181) MRAS (blue numbering). An additional resonance, presumably a split of Ile31, is present in the G22V spectrum and to a lesser extent Q71L. Intensity of this peak increases at 37˚C (blue, G22V; inset is 1D projections). **c** A fivefold molar excess of BRAF RBD added to ^{13}C-Ileδ1 wild-type MRAS (left) does not induce chemical shift changes and all 13 Ile are detected (blue numbering). RBD binding is observed with MRAS^{G22V}-GDP through multiple chemical shift perturbations (CSPs; arrows, gray). RBD binding to MRAS^{Q71L}-GDP is revealed by a characteristic peak also observed with GMPPNP-bound protein (red, arrow). This peak is visible when RBD is added to G22V but is less intense (requiring a higher contour level (blue), arrow).

GDP-bound protein was weakly retained in the SMP complex, though not to the same extent as GMPPNP-loaded MRAS^{Q71L} (Fig. 4b). As retention through a gel filtration column is stringent and requires high affinity complexes, we next formed the SMP complex on beads and quantified bound proteins following several washes. This approach revealed that MRAS^{WT} is retained in the SMP complex

whether GDP or GMPPNP bound, but the activated state interacts with significantly higher affinity (Fig. 4c). Conversely, MRAS^{Q71L} nucleated SMP formation independent of bound nucleotide (Fig. 4d). It is therefore evident that in vitro characterization of MRAS has been complicated by use of synthetic mutants and artificial loading with GMPPNP.
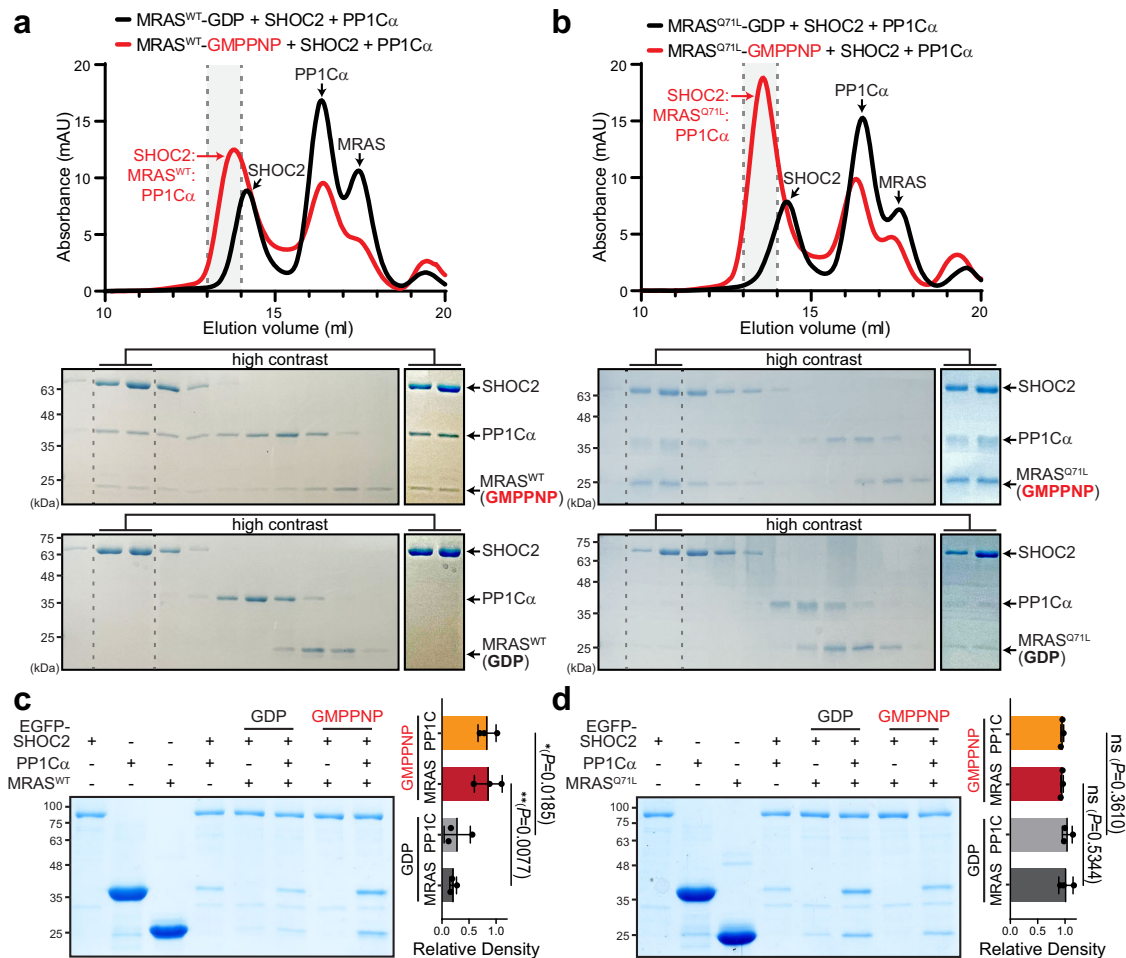
Fig. 4 | MRAS^Q71L nucleates formation of the SHOC2-MRAS-PP1Cα (SMP) complex when GDP bound. a Traces (UV 280 nm) from size exclusion chromatography (SEC) of complexes formed by MRAS^WT-GDP (black) or MRAS^WT-GMPPNP (red) with purified SHOC2 and PP1Cα. Coomassie stained SDS-PAGE gels of the corresponding fractions are below. Two fractions from the most intense SHOC2 peaks (within dashed lines) are shown to the right with higher contrast. $n = 3$ experiments were performed independently with similar results. **b** UV traces following SEC of complexes formed by MRAS^Q71L-GDP (black) or MRAS^Q71L-GMPPNP (red) with purified SHOC2 and PP1Cα. Coomassie stained gels of the corresponding fractions are below. Two fractions from the most intense SHOC2 peaks (dashed lines) are shown at right with increased contrast. $n = 3$ experiments were performed independently with similar results. **c** Nucleation of the SMP complex by MRAS^WT is significantly enhanced by GMPPNP-loading. In vitro pull-down assays mixed 12 μM each of

recombinantly purified PP1Cα and MRAS^WT with GFP-SHOC2 purified from HEK 293T cells on NHS-beads conjugated with anti-GFP nanobodies. The GTPase was preloaded with the nucleotides indicated in legend. $n = 3$ experiments were performed independently, used to calculate the relative amounts of PP1Cα/MRAS^WT precipitated by SHOC2 at right by densitometry. Plotted are mean ± standard deviation. **d** MRAS^Q71L can nucleate SMP complex formation independent of its nucleotide loaded state. In vitro pull-down assays mixed 12 μM each of purified PP1Cα and MRAS^Q71L with GFP-SHOC2 on beads. The GTPase was preloaded with the indicated nucleotides. $n = 3$ experiments were performed independently, used to calculate the relative amounts of PP1Cα/MRAS^Q71L precipitated by SHOC2 at right. Plotted are mean ± standard deviation. Statistical comparison between GDP and GMPPNP complex nucleation was performed using a 1-way ANOVA. Source data are provided as a Source Data file.

The MRAS exchange defect is complex

Given the high degree of homology between MRAS and archetypal H/K/NRAS GTPases, its inability to become activated opens a fundamental question regarding the molecular determinants of nucleotide cycling. Indeed, elucidation of residues preventing MRAS GTP-loading could drive new thinking on KRAS inhibition. As there are few amino acid substitutions in the MRAS G-domain compared to H/K/NRAS (Fig. 5a and Supplementary Fig. 4a, b), we expected identification of the contributing residues/regions would be straightforward. One amino acid conserved in all MRAS orthologs is Asp/Glu21, which is an Ala/Gly in H/K/NRAS and RRAS GTPases. This residue is in the p-loop, responsible for nucleotide coordination in classical RAS and lies in close proximity to the γ-phosphate of GTP. Otherwise, only a Pro substitution at residue 40 of the switch 1 region (Asp30 in KRAS) was a conserved change within 5 Å of the nucleotide pocket. We therefore purified MRAS variants D21A and P40D while also generating nine chimeras that incorporated large

regions of KRAS into MRAS equivalent sites, along with an N-terminal truncation that removes an extra 10 amino acids found in MRAS (Fig. 5b). RT-NMR was used to monitor nucleotide exchange of all variants and was performed with uniformly ^15N-labeled proteins incubated in 10:1 excess GTPγS for 12 h. The D21A substitution resulted in only 8% of the protein becoming GTPγS-loaded, with neither the P40D mutant or N-terminal deletion showing any exchange activity (Fig. 5c and Supplementary Fig. 5a). For the chimeras, swapping the extensive C-terminal region of KRAS (residues 80-170) into MRAS had no impact, and significant improvement in exchange was only observed by substitution of the entire p-loop to switch 2 region (MRAS^21–86 to KRAS^11–76). This chimera was 40% GTPγS loaded, still significantly lower than expected for a fully functioning RAS GTPase (KRAS is 90% GTPγS loaded in the same condition). Thus, the exchange defect in MRAS does not appear dependent on a single amino acid substitution but rather a complex interplay between multiple discrete regions.
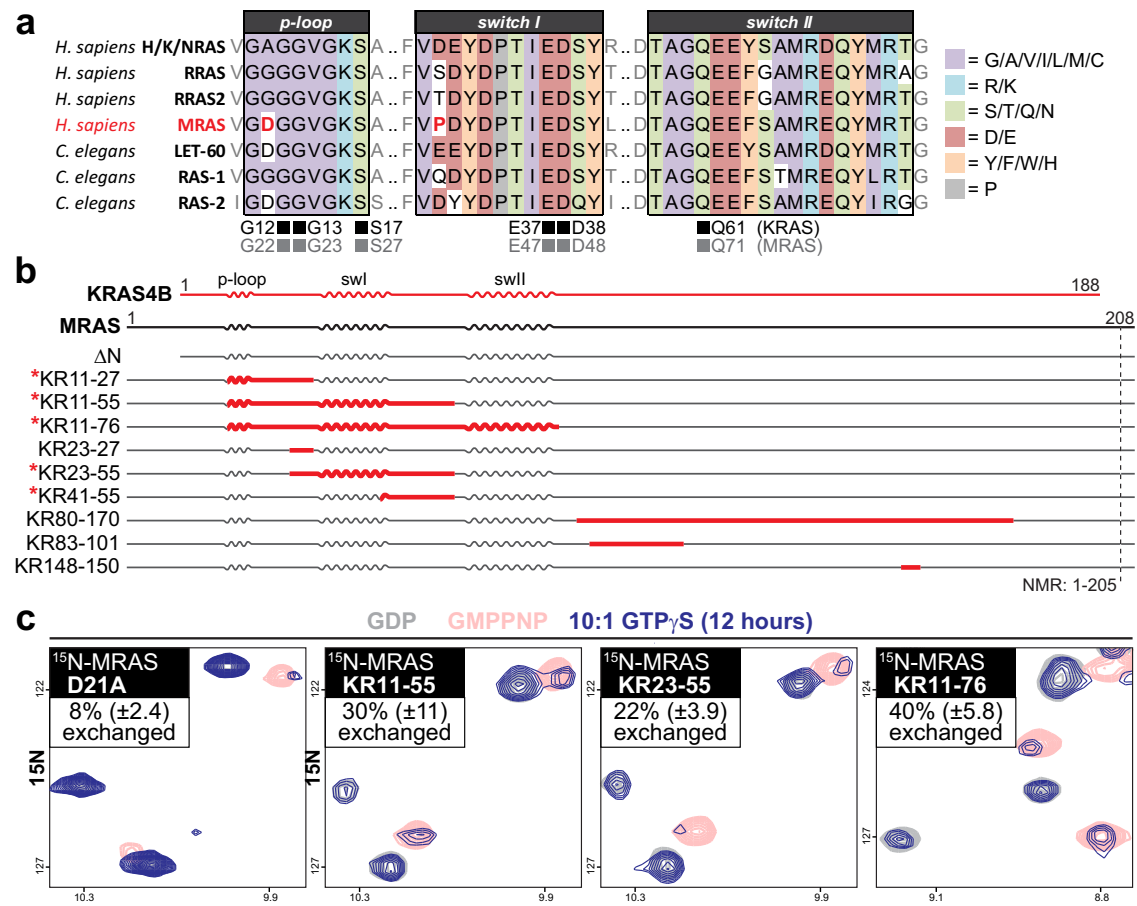
Fig. 5 | The MRAS GDP-to-GTP exchange defect is complex and only substantial amino acid substitutions rescue activity. a Sequence alignment of human RAS proteins with *C. elegans* orthologs covering the p-loop, switch 1 and switch 2 regions. Key residues from H/K/NRAS studies including frequent sites of oncogenic mutation are at bottom (human numbering). **b** Schematic representation of substitutions made in MRAS-KRAS chimeras. KRAS regions are denoted in red and MRAS in black, naming of chimeras includes amino acid numbers of KRAS used in the substitution. Red asterisks denote chimeric constructs that showed any GDP-to-GTPγS exchange. **c** Overlay of $^1H/^{15}N$ HSQC spectra from three MRAS-KRAS chimeric constructs and the point mutant MRAS^{D21A}. Spectra from ^{15}N-MRAS variants preloaded with GDP (gray) or GMPPNP (pink) are in the background with an HSQC taken 12 h after incubation with 10:1 molar excess GTPγS on top (blue). Multiple peak intensities were used to determine % exchanged (GTPγS loaded).

MRAS does not become GTP-loaded in cells

While the in vitro data clearly demonstrate MRAS is incapable of GDP-to-GTP exchange, it is possible that unknown cellular components could drive activation in cells. This is unlikely to be a GEF, as they increase the rate of nucleotide release but do not actively load proteins with GTP. We first considered whether MRAS may be post-translationally modified (PTM; e.g. phosphorylation) and used mass spectrometry to identify sites. No PTMs specific to MRAS expressed and purified from HEK 293T cells were detected compared to protein from *E. coli* (Supplementary Fig. 5b, c). As another unbiased approach, we generated interactomes for both wild-type and G22V MRAS in the osteosarcoma cell line U2OS (*H/K/NRAS* wild-type) by BioID. U2OS provided a suitable model as MRAS is highly expressed in developing bones, especially osteoblasts[39]. Stable cell lines expressing doxycycline-inducible BirA*/FLAG-tagged MRAS variants were generated by lentiviral infection along with controls (BirA*/FLAG alone and BirA*/FLAG-EGFP). BirA*/FLAG-MRAS^{G22V} could be specifically precipitated by the BRAF-RBD and the tagged proteins were appropriately targeted to the plasma membrane (Supplementary Fig. 6a, b). All proteomic hits are detailed in Supplementary Data 1. Wild-type and G22V MRAS baits had completely overlapping interactomes with near-identical preys as top hits (Supplementary Fig. 6c). No novel GEFs or other regulatory proteins were present in the datasets, and we did not detect any peptides from SHOC2 or PP1Cα. This is in sharp contrast to

previous BioID elucidation of H/K/NRAS interactomes, which change substantially upon mutational activation of the GTPases[40]. Moreover, enrichment analysis of our identified hits did not reveal a RAS/MAPK signature, but rather association with RHO-mediated cytoskeletal regulation and muscle-related disorders consistent with its naming: Muscle/Microspike-RAS (Supplementary Fig. 6d). Together, these data failed to elucidate any potential mechanism for MRAS activation in cells.

Finally, we sought to directly determine the nucleotide bound to MRAS expressed in cultured human cells to corroborate the exchange defect. These are challenging experiments, done in early work with radiolabeled nucleotides and more recently using effector binding domains. As the BRAF-RBD bound to MRAS mutants independent of nucleotide, we required an alternative approach and first adapted an HPLC-based method to identify nucleotides bound to precipitated protein[41]. Venus-tagged GTPases were overexpressed in HEK 293T cells and enriched on beads, followed by protein denaturation to extract bound nucleotides. Running these extracts by ion-paired reverse-phase (IP-RP) HPLC along with GTP and GDP standards permitted nucleotide identification. To validate the assay, we first precipitated HIS-tagged variants of KRAS and MRAS expressed in bacteria (Supplementary Fig. 7a, b). This corroborated NMR results, as KRAS mutants G12V and Q61L were substantially GTP-loaded from *E. coli* (13% and 74%, respectively) while the analogous MRAS mutants G22V and
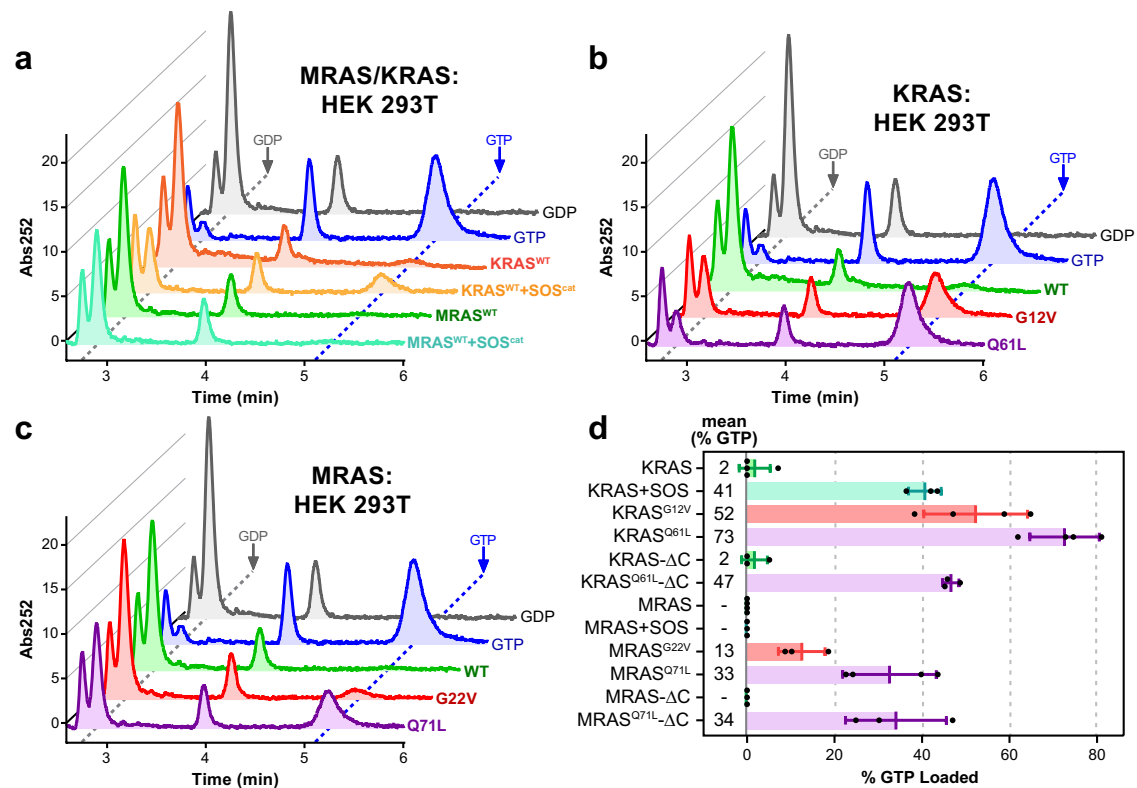
Fig. 6 | HPLC-based identification of nucleotides bound to overexpressed GTPases purified from cultured cells. a Representative chromatographs measuring UV absorbance at 252 nm for guanine nucleotides extracted from Venus-tagged RAS proteins alone or co-expressed with a membrane tethered FLAG-SOS[cat]-CaaX GEF protein (HEK 293T cells). Included are wild-type MRAS and KRAS. Proteins were purified on NHS-beads conjugated with anti-GFP nanobodies and samples heated to 95°C. Bound nucleotides were detected by IP-RP-HPLC with GDP (gray) and GTP (blue) at 5 μM serving as standards. *n* = 3 experiments were performed independently. **b** Representative chromatographs for guanine nucleotides extracted from Venus-tagged KRAS[WT], KRAS[G12V] and KRAS[Q61L] expressed in HEK 293T cells. GDP (gray) and GTP (blue) at 5 μM are standards. *n* = 3 experiments were performed independently. **c** Chromatographs of guanine nucleotides extracted from Venus-tagged MRAS[WT], MRAS[G22V] and MRAS[Q71L] expressed in HEK 293T. GDP (gray) and GTP (blue) are standards. *n* = 3 experiments were performed independently. **d** Relative amounts of guanine nucleotides extracted from Venus-tagged proteins purified from HEK 293T cells. GDP/GTP ratios were quantified from areas under the GDP- and GTP-specific curves detected by IP-RP-HPLC. Data represented are the mean and standard deviation from n=3 independent experiments. Source data are provided as a Source Data file.

Q71L remained GDP-bound. From HEK 293T cells we first examined whether the catalytic domain of SOS tethered to the plasma membrane[42] may stimulate exchange of wild-type KRAS or MRAS (Fig. 6a). SOS[cat]-CaaX increased GTP-loading of KRAS[WT] from 2% to 41% (Fig. 6d) but we observed no GTP co-precipitating with MRAS[WT] in the presence or absence of SOS. We next assayed the KRAS mutants G12V and Q61L and found they are 52% and 73% GTP-loaded from cells, respectively (Fig. 6b). As the first evidence that MRAS may become GTP-loaded, we could detect GTP fractions for both MRAS[G22V] (13%) and MRAS[Q71L] (33%) (Fig. 6c). To determine if membrane tethering was required, Venus-tagged KRASΔC and MRASΔC proteins (lacking HVR) were expressed and precipitated from HEK 293T cells. KRAS[Q61L] was 33% GTP-loaded and MRAS[Q71L] remained 34% GTP-bound (Supplementary Fig. 7c, d). While the results for KRAS are supported by all previous biochemical data, this was not true of MRAS. We were concerned the large N-terminal Venus tag, required for affinity purification, may impact nucleotide loading. To resolve this, we expressed MRASΔC wild-type and Q71L with a C-terminal Venus tag and repeated the HPLC experiments. While MRAS[WT]ΔC co-precipitated with GDP irrespective of tag position, MRAS[Q71L]ΔC with a C-terminal tag did not bind GTP and even bound poorly to GDP (Supplementary Fig. 7d). In addition to concerns about the tag, there were numerous additional proteins co-precipitating with GTPase targets (Supplementary Fig. 7e). Identification of proteins in two consistently co-purifying bands by mass spectrometry revealed enrichment of 14-3-3 isoforms and numerous RAS GTPases, predominantly of the RAB family

(Supplementary Fig. 7f). Therefore, while the HPLC assay offered some preliminary evidence that MRAS mutants may be partially GTP-loaded in cells (though not MRAS[WT]), several issues led us to derive a more direct method to observe nucleotide binding.

Use of NMR to observe proteins in their native environment, In-Cell NMR (IC-NMR), is becoming more prevalent and was recently used to characterize KRAS activation[43]. While not yet possible to obtain NMR spectra of GTPases tethered to the plasma membrane, our HPLC results suggested quantification of nucleotides bound to ΔHVR mutant proteins would inform on their capacity to become activated in cells. For this, we first optimized electroporation of bacterially-expressed MRAS[WT]ΔC with an added N-terminal FLAG tag into HEK 293T cells. Consistent concentrations of ~25−50 μM could be achieved in 500 μl samples used for NMR (cells plus rich media; Supplementary Fig. 8a, b) and, as expected, the ΔC proteins were localized generally in the cytosol (Supplementary Fig. 8c). No leakage of electroporated proteins was observed over the standard course of an NMR experiment (Supplementary Fig. 8d) and cells were typically 80−90% viable after removal from the magnet. To monitor nucleotide binding, ^{13}C-Ileδ1-labeled proteins were purified from *E. coli*, the 6xHIS-tag cleaved and GTPases loaded with GDP prior to electroporation. KRAS served as a control, and we could observe its activation by measuring intensity of the GTP- and GDP-specific chemical shifts of Ile21. IC-NMR spectra of KRAS[WT]ΔC in living cells resolved this protein remained GDP-bound (Fig. 7a, c). Conversely, KRAS[Q61L]ΔC had peaks representing both the GDP- and GTP-bound states, revealing the oncoprotein does indeed
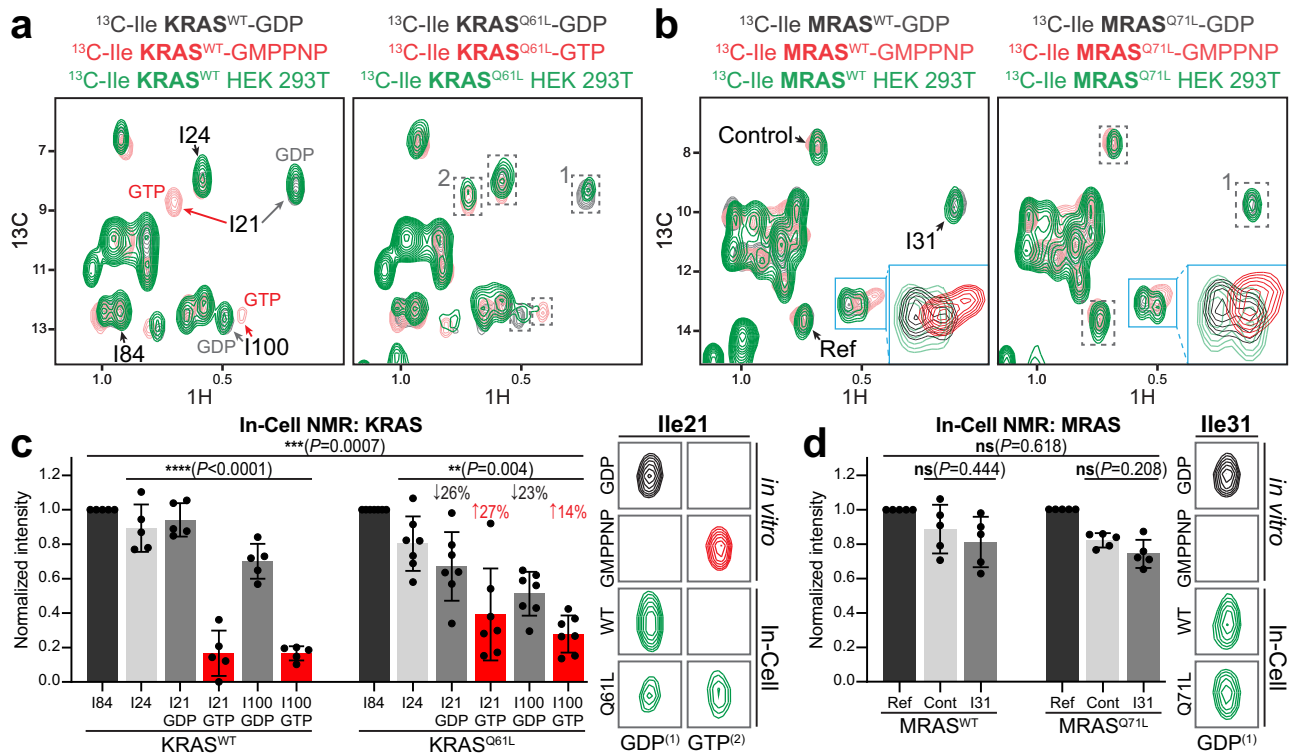
Fig. 7 | In-Cell NMR reveals MRAS^WT and MRAS^Q71L remain GDP bound in cells, in contrast to KRAS^Q61L which becomes GTP loaded. a Overlay of ^{1}H/^{13}C SOFAST-HMQC spectra from ^{13}C-Ileδ1-KRAS^WT (left) and KRAS^Q61L (right). Spectra from KRAS prebound to GDP (black) or GMPPNP/GTP (red) in buffer are in the background, and in HEK 293T cells seven hours after electroporation on top (green). Ile21 and Ile100 serve as reporting peaks for nucleotide-bound status and are emphasized with red and gray arrows for GTP and GDP, respectively, on KRAS^WT spectra and boxed on KRAS^Q61L spectra. Ile84 served as a normalization peak to permit comparisons over multiple experiments. **b** Overlay of spectra from ^{13}C-Ileδ1-MRAS^WT (left) and MRAS^Q71L (right) preloaded with GDP (black) or GMPPNP (red) in solution, or in HEK 293T cells seven hours after electroporation (green). Presumed MRAS Ile31 (corresponding with KRAS Ile21) is marked. Broadening of Ile31 informs on GDP/GTP loading, as does the line shape of peaks within the blue square (zoomed, inset). 'REF' peak was for normalization between biological replicates. **c** Quantitation of GDP- and GTP-bound fractions of KRAS^WT and KRAS^Q61L in cells.

Ile84 was used for normalization. Ile24 is also unchanged by nucleotides and is a control. Data are mean and standard deviation from $n = 3$ independent experiments. Statistical comparison between wild-type and mutant used a 2-way ANOVA ($P = 0.0007$) with a 1-way ANOVA for in-group comparisons (wild-type $P < 0.0001$ and Q61L $P = 0.004$). At right are resonances observed at Ile21 GDP- and GTP chemical shifts (marked with a 1 and 2 on spectra in **a**). **d** Quantitation of peak intensity for MRAS^WT (left) and MRAS^Q71L (right) in HEK 293T cells. Loss of the GDP-specific peak reports on GTP loading. 'REF' is stable independent of nucleotide and was used for normalization. Control peak is also unchanging. Data are mean and standard deviation from at least $n = 3$ independent experiments. Statistical analysis between wild-type and mutant used a 2-way ANOVA ($P = 0.618$) and in-group comparisons used t tests (wild-type $P = 0.444$ and Q71L $P = 0.208$). At right are resonances at the Ile31 (GDP) chemical shift (marked with a 1 on spectra in **b**). Source data are provided as a Source Data file.

become activated in cells. Similar experiments were then performed with wild-type and Q71L MRASΔC, and we monitored activation in cells by quantifying intensity (broadening) of the GDP-specific Ile31 peak (a second Ile served as an internal control). This revealed no difference between wild-type and Q71L MRASΔC, with both remaining completely GDP-loaded (Fig. 7b, d). This direct observation of RAS nucleotide binding supports the premise that MRAS is incapable of nucleotide exchange, in vitro or in cells, compared with classical RAS GTPases.

Discussion

Our understanding of small GTPase function is derived from work on a subset of these proteins, particularly archetypal H/K/NRAS. Most RAS GTPases are thus believed to cycle between GDP-bound 'inactive' and GTP-bound 'active' conformations. To achieve this requires similar affinities for guanine nucleotides, which drives activation upon nucleotide release due to an excess of GTP in cells. More careful biochemical characterization of RAS superfamily GTPases is revealing some are not canonical switch-like proteins and these are now being classified as pseudoGTPases[7]. Here, we reveal the close H/K/NRAS homolog MRAS is unable to intrinsically exchange GDP-to-GTP even upon addition of SOS. The enzyme works in reverse exchange assays, confirming it is functional but has high affinity for GDP. Interestingly,

neither the N-terminal extension of MRAS or conserved substitutions in the p-loop or switch 1 regions were entirely causative of the exchange defect. As a distal ortholog from nematode worms displayed the same anomaly, it appears this is a conserved feature. It is likely that loss of GTP binding in an early ortholog made further amino acid substitutions that disrupt GTP-loading permissible, and it may ultimately be difficult to isolate the molecular basis of the defect. Nevertheless, this is an intriguing question as the high sequence conservation between MRAS and H/K/NRAS suggests a potential pathway to inhibit activation of RAS oncoproteins.

A complicating factor in previous work on MRAS has been use of RAS-based activating mutants and in vitro GMPPNP loading. Indeed, loading small GTPases with GMPPNP is simplified by use of phosphatases that eliminate competing GDP. A crystal structure of activated MRAS was solved using this approach[44], as were the recently published SMP complex structures. Comparison between GDP- and GMPPNP-loaded MRAS shows remarkable differences in nucleotide-driven structural changes compared to other RAS proteins. While the switch 2 region of HRAS swings out upon GMPPNP loading and switch 1 remains relatively stable, MRAS demonstrates the reverse (Fig. 8). B-factors suggest the MRAS switch 1 region is highly mobile and it swings away from GMPPNP while the switch 2 region is more fixed. This
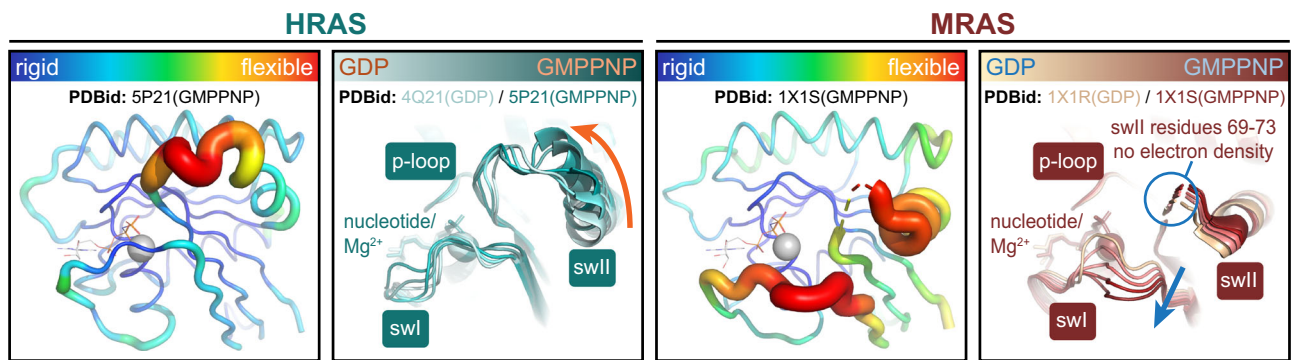
HRAS   MRAS

Fig. 8 | Nucleotide-driven structural conversions in KRAS versus MRAS. Structural comparison of GDP- and GMPPNP-loaded HRAS (left panels) and MRAS (right panels), focusing on flexibility of the p-loop, switch 1 and switch 2 regions. Putty representations for HRAS-GMPPNP (PDBid: 5P21) and MRAS-GMPPNP (PDBid: 1X1S) are colored by crystallography B-factors (blue=rigid to red=-flexible). Ribbons diagrams are overlays of GDP- and GMPPMP-bound proteins with three simulated steps to represent motion. MRAS switch 2 residues 69-73 have no electron density.

is likely why Ile21 of KRAS is visible in our $^{1}H/^{13}C$ NMR spectra for both GTP- and GDP-bound states, while Ile31 of MRAS-GMPPNP is broadened beyond detection and only loss of the GDP-specific resonance reports on GTP loading. Most concerning is the capacity for MRAS G22V and Q71L mutants to bind effectors in the GDP-bound state. Our ^{31}P-NMR experiments clearly show MRAS^{G22V}-GDP exists in a 2-state equilibrium and the activated state is stabilized by RBD binding. This was not observable for MRAS^{Q71L}, likely due to lower affinity and the high protein concentrations required for ^{31}P-NMR, but ^{1}H-^{13}C correlation experiments confirmed that MRAS^{Q71L} can complex with the RBD when GDP-bound. Further experiments with SHOC2 and PP1Cα verified this mutant can also nucleate SMP formation when loaded with GDP. The initial identification of SHOC2 as an MRAS interactor was done using the Q71L variant[11], and clear data on whether wild-type MRAS can be GTP-loaded and mediate SMP formation in cells is required.

Current interest in MRAS and the SMP complex as therapeutic targets is derived from their potential role in activating the MAPK pathway, however, several lines of evidence suggest MRAS may not be the major GTPase involved in SMP formation. The first is that H/K/NRAS can substitute for MRAS and bind SHOC2-PP1Cα, at slightly reduced affinities, driving dephosphorylation of RAF to a similar extent as MRAS[21]. Second, we identified *SHOC2* orthologs in all metazoans including early animals such as sponges and cnidarians (Supplementary Fig. 9a). Conversely, early animals do not have *MRAS* orthologs and numerous complex organisms have lost this gene, including the model fruit fly *D. melanogaster*. Third, data from DepMap that uses CRISPR knockouts to resolve genetic relationships suggests there is no co-dependency between *MRAS* and any genes encoding proteins involved in MAPK signaling (Supplementary Fig. 9b). This is in contrast to *SHOC2*, which shows co-dependency with numerous MAPK genes including *RAF1*, *KRAS*, *NF1* and *SOS1*. Moreover, synthetic lethality with MEK inhibitors is observed with *SHOC2* but not *MRAS*[21,45] and knockdown of MRAS does not influence CRAF^{S259} dephosphorylation, whereas SHOC2 knockdown does[14]. These data are supported by our BioID interactomes which offered no evidence that MRAS is implicated in RAS/MAPK signaling, and collectively imply that MRAS is not essential for SHOC2-PP1Cα holoenzyme formation.

Finally, complete biochemical characterization of protein function should now be requisite for all experiments with small GTPases. Such investigations have been common for over three decades, but we still lack biochemical data for most RAS superfamily proteins. This includes nucleotide cycling kinetics in addition to structures, preferably using methods that directly monitor GTPase conformation rather than detection of free nucleotides. Unfortunately, this is the case with our HPLC-based assays which offered the only evidence that

MRAS mutants might be partially GTP-loaded in cells. The indirect nature of the assay means we cannot decipher whether signals were from MRAS or co-precipitating proteins, and additional complications are created by the affinity tag, lysis and purification. IC-NMR offered a superior approach to determine bound nucleotides as the proteins were untagged, the cells intact, and the signals report on atomic-level nucleotide interactions in a highly quantitative manner. This method verified MRAS^{WT} remains GDP-loaded and clearly contrasted KRAS^{Q61L} with its analogous mutant MRAS^{Q71L}. Nevertheless, we remain open to the notion that our HPLC analyses are accurately reporting MRAS^{Q71L} nucleotide loading though it is difficult to reconcile how this is achieved. Only a subcellular locale completely lacking GDP or an active loading mechanism for GTP, perhaps concurrent with an effector, could result in classical MRAS activation. There are no data suggesting this a likely scenario, but how this could function may be a focus of future work. There is little doubt that more pseudoGTPases will be identified, and the mechanisms by which such proteins control signaling networks in the absence of canonical switching is an important and completely open question.

Methods
Plasmid constructs and antibodies
Gateway entry vectors encoding mutationally activated human small GTPases KRAS4B (GeneID: 3845), RRAS (GeneID: 6237), RRAS2 (GeneID: 22800), MRAS (GeneID: 22808) and CDC42 (GeneID: 998) were a kind gift from Dr. Jean-François Côté (IRCM, Montreal). These were shuttled into mammalian expression vectors with N-terminal Venus-tags. For proteomic analysis we generated BirA*/FLAG-tagged mammalian expression constructs by shuttling MRAS^{WT} and MRAS^{G22V} into the N-pSTV6 BioID expression vector, a kind gift from Dr. Anne-Claude Gingras (LTRI, Toronto). Second generation lentiviral packaging and envelope expression vectors psPAX2 and pCMV-VSV-G were used to generate cell lines[46]. For bacterial expression, KRASΔC (1-171), MRAS (1-205), MRASΔC (1-181) and the SOS^{cat} domain of human SOS1 (residues 564–1049) were cloned into pET-15b (Novagen/EMD Biosciences) with an N-terminal polyhistidine (6xHIS) tag. *C. elegans* LET-60 (GeneID: 178104) and RAS-2 (GeneID: 175625) were synthesized as Gateway entry vectors containing a thrombin cleavage site (Bio Basic) and shuttled into pDEST17 which encodes an N-terminal polyhistidine (6xHIS) tag. MRAS/KRAS chimeric proteins were synthesized and cloned directly into pET-15b (Bio Basic). RRAS and RRAS2 Gateway entry clones were shuttled into pDEST17 and a thrombin site was subsequently cloned to permit cleavage of the tag. For BRAF RBD expression, the RBD of BRAF (150-233; GeneID: 673) was cloned into pGEX-4T2 (Amersham Pharmacia Biotech), a bacterial expression vector with an N-terminal Glutathione *S*-transferase (GST) tag. Point

mutations and deletions were performed by site-directed mutagenesis. pGBHPS-MSP which encodes the membrane scaffold protein (MSP) variant 1D1 (MSP1D1) was a gift from Dr. Mitsu Ikura's lab[32]. Full length SHOC2 was cloned into pDEST-pcDNA3-TEV-Venus-5′. Full length PP1Cα was cloned into pET-28 with an N-terminal polyhistidine (6xHIS) tag (EMD Biosciences). pGRO7 plasmid, encoding GroEL/GroES (Takara Bio), was used as chaperone for PP1Cα expression. Supplementary Data 2 lists all primers used in the study. Antibodies used: anti-GFP (Abcam, ab290; WB: 1:5000), anti-FLAG M2 (Sigma, F3165; IF: 1:100; WB: 1:1000), rabbit anti-FLAG (Sigma F7425; IF:1:200), anti-phospo-ERK1/2 (Cell Signaling, 9101; WB: 1:1000), anti-ERK1/2 (Cell Signaling, 4695; WB: 1:1000), goat anti-rabbit IgG (H + L), Alexa-Fluor 647 (Life Technologies A21244; IF 1:200), goat anti-rabbit IgG (H + L), Alexa-Fluor 555 (Life Technologies A21428; IF 1:500), HRP-conjugated anti-rabbit (Cedarlane, NA934; WB: 1:10000) and HRP-conjugated anti-mouse IgG (Fisher, 45-000-679; WB: 1:10000).

Mass spectrometry

BioID[47,48] was done using U2OS cells (ATCC HTB-96) stably expressing BirA*/FLAG-tagged MRAS fusion proteins grown in 2×150 cm^2 plates of sub-confluent cells (60%) incubated 24 h in complete media supplemented with 1 μg/ml doxycycline (BioShop) and 50 μM biotin (Bio Basic). Cell pellets were resuspended by pipetting up and down and vortexing in 1.5 ml of RIPA buffer (50 mM Tris-HCl pH 7.5, 150 mM NaCl, 1% NP-40, 1 mM EDTA, 1 mM EGTA, 0.1% SDS, protease inhibitors (Sigma), and 0.5% sodium deoxycholate). 1 μl of benzonase (250U) was added to each sample and the lysates sonicated on ice. Lysates were centrifuged for 20 min at 12,000 × g and then incubated with streptavidin-sepharose beads (GE) pre-washed with RIPA buffer. Affinity purification was performed at 4 °C on a nutator for 3 h, beads were pelleted (400 x g, 1 min), the supernatant removed and beads washed 3 times in 1 ml RIPA buffer followed by 3 times in 1 ml 50 mM ammonium bicarbonate pH 8.0 (ABC). Residual ABC was removed, and beads were resuspended in 100 μl of 50 mM ABC for protein digestion. 10 μl of a 0.1 μg/μl trypsin stock (resuspended in 20 mM Tris-HCl, pH 8) was added for a final concentration of 1 μg of trypsin and incubated at 37 °C overnight. The following day, an additional 1 μg of trypsin was added (in 10 μl of 20 mM Tris-HCl, pH 8.0) and the samples incubated an additional 2–4 h. Beads were pelleted (400 × g, 2 min) and the supernatant (peptides) transferred to a fresh 1.5 ml tube. Beads were rinsed 2 times in 100 μl HPLC water and pooled with the collected supernatant. Formic acid was added to a final concentration of 2% to end digestion (30 μl of 50% stock). The pooled supernatant was centrifuged at 10,000 × g for 10 min, the supernatant collected and lyophilized. Peptides were resuspended in 5% formic acid and one quarter of the sample was analyzed per MS run. 5 μl of each sample was directly loaded at 400 nl/min onto a 75 μm × 12 cm emitter packed with 3 μm ReproSil-Pur C$_{18}$-AQ. The peptides were eluted from the column over a 90 min gradient generated by a NanoLC-Ultra 1D plus (Eksigent) nanopump and analyzed on a TripleTOF™ 5600 instrument (AB SCIEX). The gradient was delivered at 200 nL/min starting from 2% acetonitrile with 0.1% formic acid to 35% acetonitrile with 0.1% formic acid over 90 min followed by a 15 min clean-up at 80% acetonitrile with 0.1% formic acid, and a 15 min re-equilibration period in 2% acetonitrile with 0.1% formic acid for a total of 120 min. To minimize carryover between each sample, the analytical column was washed for 3 h by running an alternating sawtooth gradient from 35% acetonitrile with 0.1% formic acid to 80% acetonitrile with 0.1% formic acid, holding each gradient concentration for 5 min. Analytical column and instrument performance were verified after each sample by loading 30 fmol BSA tryptic peptide standard (Michrom Bioresources Inc.) with 60 fmol α-Casein tryptic digest and running a short 30 min gradient. TOF MS calibration was performed on BSA reference ions before running the next sample in order to adjust for mass drift and verify peak intensity. The instrument method was set to a discovery or IDA mode which consisted of

one 250 ms MS1 TOF survey scan from 400-1300 Da followed by twenty 100 ms MS2 candidate ion scans from 100 to 2000 Da in high sensitivity mode. Only ions with a charge of 2+ to 4+ which exceeded a threshold of 200 cps were selected for MS2, and former precursors were excluded for 10 s after 1 occurrence. MS data generated by TripleTOF™ 5600 were stored, searched and analyzed using the Pro-Hits laboratory information management system (LIMS) platform[49]. Within ProHits, the resulting WIFF files were first converted to an MGF format using WIFF2MGF converter and to an mzML format using ProteoWizard[50] (v3.0.4468) and the AB SCIEX MS Data Converter (V1.3 beta) and then searched using Mascot (v2.3.02) and Comet (v2012.02 rev.0). The spectra were searched with the human and adenovirus complements of the RefSeq database (version 57) from NCBI supplemented with "common contaminants" from the Max Planck Institute and the Global Proteome Machine (GPM; http://www.thegpm.org/crap/index.html). Parameters included: fully tryptic cleavages, allowing up to 2 missed cleavage sites per peptide. The mass tolerance was 40 ppm for precursors with charges of 1+ to 3+ and a tolerance of ±0.15 amu for fragment ions. Variable modifications were deamidated asparagine and glutamine and oxidized methionine. The results from each search engine were analyzed through TPP (the Trans-Proteomic Pipeline[51], v4.6 OCCUPY rev 3) via the iProphet pipeline[52]. Two unique peptide ions and a minimum iProphet probability of 0.95 were required for protein identification prior to analysis with SAINTexpress version 3.3[53]. Eight control runs were used for comparative purposes: 4 runs of a BioID analysis conducted on cells expressing the BirA*/FLAG tag only to control for non-specific biotinylation of intracellular proteins, and 4 runs from a BioID analysis conducted on an unrelated bait protein (EGFP) to mimic the condition in which endogenous biotinylation (which primarily occurs on mitochondrial carboxylases) would be predominant. Each negative control was analyzed in biological replicates with 4 independent biological replicates per type of control (i.e. not simple re-injections or technical replicates). A compression strategy using SAINTexpress collapsed the 8 controls to the highest 4 spectral counts for each hit, helping to capture spurious binding behavior of some contaminants. Thus, each potential prey across the 2 biological replicates of the bait is assessed for significance across the 4 highest values across the 8 controls we used. All hits are reported in Supplementary Data 1 with SAINT score as a confidence measure. Only proteins passing a statistical threshold of FDR ≤ 0.1 were deemed high quality interactions in Supplementary Fig. 6.

For in-gel digests, bands were destained in 50% MeOH (Sigma-Aldrich). Each band was shrunk in 50% acetonitrile (ACN), reconstituted in 50 mM ammonium bicarbonate with 10 mM TCEP [Tris(2-carboxyethyl)phosphine hydrochloride; Thermo Fisher Scientific], and vortexed for 1 h at 37 °C. Chloroacetamide (Sigma-Aldrich) was added for alkylation to a final concentration of 55 mM. Samples were vortexed for another hour at 37 °C. One microgram of trypsin was added, and digestion was performed for 8 h at 37 °C. Peptide extraction was conducted with 90% ACN. The extracted peptide samples were dried down and solubilized in 5% ACN-0.2% formic acid (FA). The samples were loaded on a C4 guard column (Optimize Technologies) connected directly to the switching valve. They were separated on a home-made reversed-phase column (150-μm i.d. by 180 mm) with a 56-min gradient from 10 to 30% ACN-0.2% FA and a 600-nl/min flow rate on a Easy-nLC 1200 connected to an Orbitrap Exploris 480 (Thermo Fisher Scientific, San Jose, CA). Each full MS spectrum acquired at a resolution of 120,000 was followed by tandem-MS (MS-MS) spectrum acquisition for a maximum of 3 s on the most abundant multiply charged precursor ions. Tandem-MS experiments were performed using higher energy collisional dissociation (HCD) at a collision energy of 34%. The data were processed using PEAKS X Pro (Bioinformatics Solutions, Waterloo, ON) and a Uniprot human database. Mass tolerances on precursor and fragment ions were 10 ppm and 0.3 Da, respectively. Variable selected posttranslational modifications were

carbamidomethyl (C), oxidation (M), deamidation (NQ), acetyl (N-ter) and phosphorylation (STY).

Purification of recombinant proteins

RAS GTPases and BRAF RBD: For unlabeled proteins, GST- or 6xHIS-tagged proteins were expressed in *Escherichia coli* (BL21-DE3-codon +) cells and grown in LB media at 37 °C. Cells were induced with 0.2 mM IPTG at OD_{600} 0.9 and grown at 18 °C overnight. Proteins encoded in pDEST17 vector were transformed in BL21-A1 cells and grown in LB media at 37 °C. Cells were induced with 0.2% (w/v) L-arabinose at OD_{600} 0.9 and grown at 22 °C overnight. Uniformly labeled ^{15}N proteins were expressed similarly, but using an M9 minimal medium supplemented with 1 g/L $^{15}NH_4Cl$. Selectively labeled ^{13}C-Ileδ1 methyl proteins were grown in M9 minimal medium supplemented with 1 g/L NH_4Cl. ^{13}C-Ileδ1 methyl was added 1 h before induction. Cells were lysed using sonication in 20 mM Tris-HCl (pH 7.5), 150 mM NaCl, 5 mM $MgCl_2$, 10% (v/v) glycerol, 0.4% (v/v) NP-40, protease inhibitors, and either 1 mM DTT or 5 mM β-mercaptoethanol. Lysates were cleared by centrifugation and incubated with Ni-NTA or GSH resin for 1–2 h at 4 °C. After binding, resins were washed using a high-salt buffer (20 mM Tris-HCl (pH 7.5), 500 mM NaCl, 5 mM $MgCl_2$, and 1 mM DTT or 5 mM β-mercaptoethanol), followed by a low salt buffer (20 mM Tris-HCl (pH 7.5), 150 mM NaCl, 5 mM $MgCl_2$, and 1 mM DTT or 5 mM β-mercaptoethanol). HIS-tagged proteins were eluted with 300 mM imidazole followed by thrombin cleavage. GST-tagged proteins were either cleaved with thrombin directly on resin overnight at 4 °C or eluted using 30 mM reduced glutathione. Proteins were further purified by size exclusion chromatography (SEC) using an S75 column (GE). *Nucleotide Exchange of GTPases:* Purified GTPases were incubated with a tenfold molar excess (nucleotide:protein) of guanosine 5′-[β,γ-imido]triphosphate (GMPPNP, Sigma Aldrich), guanosine 5′-[γ-thio]triphosphate (GTPγS, Sigma Aldrich) or GTP along with 10 mM EDTA at 37 °C for 10 min. For exchanges using GMPPNP calf intestinal phosphatase (CIP) was used to hydrolyse existing nucleotide. 20 mM $MgCl_2$ was added, and samples were incubated on ice for 10 min. Buffer exchange was performed using a S75 column (GE). For hydrolysis assays, aliquots of GTP-loaded GTPases were flash frozen and stored at −80 °C until use. In order to exchange MRAS with GTP, all GDP nucleotide had to be hydrolyzed using CIP, as in the presence of GDP MRAS will not undergo exchange. To this end, purified protein was first exchanged with GMPPNP as previously described, followed by a second exchange using 20-fold molar excess (nucleotide:protein) of GTP. *PP1Cα:* Full-length PP1Cα was co-transformed with the pGRO7 plasmid encoding GroEL/GroES (Takara Bio) into BL21(DE3) cells (Thermo Fisher). Cells were grown in LB media with 50 µg/ml ampicillin, 34 µg/ml chloramphenicol, 1 mM $MnCl_2$ and 0.1% (w/v) L-arabinose to an OD_{600} of 0.7. Cells were induced with 0.25 mM IPTG and grown at 18 °C overnight. The cells were collected and stored at -80 °C. Cell pellets were resuspended in 40 ml of PP1Cα lysis buffer (20 mM Tris-HCl (pH 7.5), 700 mM NaCl, 10% (v/v) glycerol, 0.4% (v/v) NP-40, 5 mM $MgCl_2$ and 1 mM $MnCl_2$) supplemented with an EDTA-free protease inhibitor cocktail (Roche). Homogenously resuspended cells were lysed with 20 min of sonication (1 s of sonication/3 s of cooling period) with 30% power. Cell debris was removed by centrifugation at 30,000 × g for 30 min. The clarified lysate was incubated for 1 h with pre-equilibrated Ni Sepharose 6 Fast Flow (Cytiva) beads in the Econo-Column glass chromatography column (Bio-Rad). Beads were washed (20 mM Tris-HCl (pH 7.5), 700 mM NaCl, 5 mM $MgCl_2$, 1 mM $MnCl_2$ and 20 mM Imidazole) and PP1Cα eluted (20 mM Tris-HCl (pH 7.5), 700 mM NaCl, 5 mM $MgCl_2$, 1 mM $MnCl_2$ and 250 mM Imidazole). The HIS-tag was removed with thrombin protease at 4 °C overnight, and protein was injected into a pre-equilibrated Superdex 75 HiLoad 26/600 (Cytiva) for final purification into SEC buffer (20 mM Tris-HCl (pH 7.5), 700 mM NaCl, 5 mM $MgCl_2$, 1 mM $MnCl_2$ and 1 mM TCEP). The fractions containing PP1Cα protein were pooled, concentrated, and stored at -80 °C until use.

SHOC2: Full length human SHOC2 was expressed in HEK 293T cells, transiently transfected using polyethyleneimine (PEI). Cells were collected and stored as a pellet at -80 °C until purification. The cell pellet was resuspended in 40 ml of lysis buffer (50 mM Tris-HCl (pH 7.5), 600 mM NaCl, 0.5% (v/v) NP-40 and 1 mM TCEP) supplemented with EDTA-free protease inhibitor cocktail (Roche) and 0.2 mg benzonase. Homogenously resuspended cells were sonicated with three cycles of 5 s sonication with 50% power, followed by 30 s cooling periods. Cell debris was removed by centrifugation at 30,000 × g for 30 min and filtration. Clarified lysates were passed over a 5 ml HiTrap NHS-Activated column (Cytiva) pre-coupled anti-GFP/YFP nanobody[54]. The column was washed with 100 ml of wash buffer (50 mM Tris-HCl (pH 7.5), 400 mM NaCl, 0.1% (v/v) NP-40 and 1 mM TCEP) and 50 ml of low salt wash buffer (20 mM Tris-HCl (pH 7.5), 200 mM NaCl, 0.1% (v/v) TWEEN-20 and 1 mM TCEP). 2 ml of TEV elution buffer (low salt wash buffer plus TEV protease) injected to the column and incubated overnight at 4 °C. Next day, untagged SHOC2 was eluted and injected into a Superdex 200 Increase 10/300 GL (Cytiva) which had been equilibrated with SEC buffer (20 mM Tris-HCl (pH 7.5), 200 mM NaCl and 1 mM TCEP). Fractions containing SHOC2 protein were pooled, concentrated and stored at −80 °C until use. *MSP1D1:* Membrane Scaffold Protein for nanodiscs was expressed in *E. coli* (BL21-DE3-codon +) and grown in 2xYT media at 37 °C. Cells were induced with 1 mM IPTG at OD_{600} 1.0. Cells were then grown at 37 °C for one additional hour, and then at 28 °C for 2 h. Cells were resuspended in 20 mM sodium phosphate buffer (pH 7.4), 1 mM PMSF (protease inhibitor), and 1% (v/v) final Triton-X-100 was added slowly, followed by sonication. Lysates were cleared by centrifugation and incubated with Ni-NTA for 45 min at 4 °C. After binding, resins were washed with each of: Wash 1 (40 mM Tris-HCl (pH 8.0), 300 mM NaCl, 1% (v/v) Triton X-100), Wash 2 (40 mM Tris-HCl (pH 8.0), 300 mM NaCl, 50 mM sodium cholate), Wash 3 (40 mM Tris-HCl (pH 8.0), 300 mM NaCl), Wash 4 (40 mM Tris-HCl (pH 8.0), 300 mM NaCl, 50 mM imidazole). Proteins were eluted with 40 mM Tris-HCl (pH 8.0), 300 mM NaCl, and 300 mM imidazole, followed by cleavage using HRV3C. Briefly, HRV3C was added to the eluted protein and placed in dialysis tubing in 1 L buffer (20 mM Tris-HCl (pH 7.4), 100 mM NaCl, 1 mM TCEP) and kept at room temperature for 4 h with stirring, after which it was transferred to 4 °C overnight. Further purification was done by SEC using a Superdex 200 Increase 10/300 GL column (Cytiva).

Nanodisc assembly and preparation

Lipids: 1,2-dioleoyl-*sn*-glycero-3-phoshocholine (DOPC), 1,2-dioleoyl-*sn*-phospho-L-serine (DOPS) and thiol reactive lipid 1,2-dioleoyl-*sn*-glycero-3phosphoethanolamine-*N*-[4-(p-maleimidomethyl) cyclohex-ane-carboxamide] (PE-MCC) were used in a molar ratio of 15:4:1 (Avanti Polar Lipids) for a final 50 mM solution. Lipids were first dissolved in chloroform and aliquoted into glass vials with appropriate amounts to obtain 15:4:1 ratio, solvent was then removed under a stream of nitrogen gas. Lipid film was resuspended in 0.5 ml of 50% (v/v) acetonitrile solution in water and sonicated, followed by flash freezing. Frozen aliquots were lyophilized overnight and stored at −80 °C until use. *Assembly:* Lipids were dissolved in 0.25 ml of nanodisc (ND) buffer (20 mM Tris-HCl (pH 7.4), 100 mM NaCl) with 100 mM sodium cholate and transferred to 1.5 ml microfuge tube. To dissolve, lipid solutions were subjected to 5 cycles of 3 min at 45 °C, 3 min sonication, 1 min vortex, and freezing in dry ice. To the resulting solution, 500 µl of 600 µM MSP1D1 was added, and incubated at room temperature with nutation. Cholate was removed by adding Bio-Beads SM-2 adsorbents (Bio-Rad) in ND buffer and incubated at room temperature for 2 h with nutation. The mixture was quick-spun and transferred to a prewashed microfuge column placed in a 2 ml microfuge tube and allowed to filter by gravity. The column was rinsed twice with 0.125 ml ND buffer, and these were pooled with the initial flowthrough; followed by purification through gel filtration in a S200 column equilibrated with ND

buffer. Nanodisc fractions collected after SEC were concentrated to 0.5 ml for GTPase conjugation. *MRAS conjugation to nanodiscs*: A 0.5 ml aliquot of 600 μM MRAS was added to assembled nanodiscs and placed to nutate at room temperature overnight (16 hrs). The mixture was purified by SEC using an S200 column preequilibrated with ND buffer supplemented with 1 mM TCEP and 5 mM MgCl₂.

Biochemical and biophysical protein analysis

Isothermal Titration Calorimetry (ITC): Affinity between GTPases and the BRAF RBD were measured using a MicroCal ITC200 (Malvern). Protein stocks were diluted using filtered and degassed solution of 20 mM Tris-HCl (pH 7.5), 150 mM NaCl, and 1 mM DTT. Experiments were carried out at 25 °C or 30 °C. Heats of dilution were determined from control experiments in which domains were titrated into buffer alone. Data were fit using Origin 7 with Microcal-ITC (OriginLab). *Precipitation Assays:* To elucidate RBD-GTPase interactions, HEK 293T cells were seeded on 24-well plates (0.2×10⁶ cell confluency) and transiently transfected with 500 ng of DNA using PEI. U2OS cells stably expressing BirA*/FLAG-tagged MRAS or KRAS fusion proteins were induced using 1 μg/ml doxycycline. 48 h after transfection or induction, cells were harvested and lysed (20 mM Tris-HCl (pH 7.5), 150 mM NaCl, 5 mM MgCl₂, 10% (v/v) glycerol, 1% (v/v) Triton X-100, 1% (v/v) NP-40, 1 mM DTT, and protease inhibitors) and placed on ice for 10 min. The lysate was clarified by centrifugation at $21,000 \times g$ for 15 min. Supernatants were incubated with 2 μM of recombinantly purified GST-tagged RAF RBD or GST alone and glutathione beads for 30 min. The mixture was washed three times with lysis buffer (without protease inhibitors) and centrifugation, beads were then resuspended in SDS-loading buffer followed by heating. For Western blotting, protein samples were separated using SDS-polyacrylamide gel electrophoresis (SDS-PAGE) and transferred to nitrocellulose membranes. Membranes were blocked with Tris-buffered saline plus 0.1% (v/v) Tween (TBST) containing 5% (w/v) skim milk (or 3% (w/v) Bovine Serum Albumin (BSA) for phospho-protein antibodies), followed by overnight incubation with primary antibody. Detection was with HRP-conjugated anti-rabbit or anti-mouse immunoglobulin (Ig) followed by treatment with enhanced chemiluminescence reagent (Bio-Rad). Signals were detected using a Bio-Rad ChemiDoc imaging system and analyzed with ImageLab software. *GST mixing experiments*: 2.5 μM of recombinantly purified GST-tagged BRAF RBD bound to glutathione beads, or GST alone control, were incubated for 30 mins with 25 μM purified 6xHIS-GTPase, either exchanged with GDP of GMPPNP. Beads were washed three times by centrifugation using lysis buffer and were resuspended in SDS-sample buffer and separated by SDS-PAGE. *SHOC2-MRAS-PP1Cα pull-down experiments*: HEK 293T cells expressing GFP-SHOC2 were suspended in lysate buffer (20 mM Tris-HCl (pH 7.5), 150 mM NaCl, 5 mM MgCl₂, 10% (v/v) glycerol, 1% (v/v) NP-40, 1% (v/v) Triton X-100, 1 mM DTT and protease inhibitors), incubated on ice for 15 min, and cleared at $21,000 \times g$ for 10 min at 4 °C. Cleared lysate was incubated with N-hydroxysuccinimide (NHS) beads (GE17-0906-01, Cytiva) pre-conjugated with anti-GFP/YFP nanobodies. Beads were incubated for 30 mins with 12 μM purified PP1Cα and 12 μM purified GTPase, either exchanged with GDP of GMPPNP, as indicated. Beads were washed three times by centrifugation using lysis buffer and were resuspended in SDS-sample buffer and separated by SDS-PAGE. *High Pressure Liquid Chromatophraphy (HPLC):* For *E.coli* expressed proteins, purified stocks were diluted to 200 μM in 200 μL of 20 mM Tris-HCl (pH 7.5), 150 mM NaCl, 5 mM MgCl₂,1 mM DTT solution and boiled at 95 °C for 6 min followed by centrifugation at $21,000 \times g$ for 10 min. The supernatant containing released nucleotides was filtered through pre-washed PVDF centrifugal filters (0.22 μm PVDF centrifugal filter (UFC30GV25, Millipore)). For GTPases expressed in cell culture, HEK 293T cells were seeded on a 15 cm plates (5×10^6 confluency) and transiently transfected with 25 μg of plasmid DNA using PEI. 48 h after transfection, cells were harvested and lysed (20 mM Tris-HCL (pH 7.5),

150 mM NaCl, 5 mM MgCl₂, 10% (v/v) glycerol, 1% (v/v) Triton X-100, 1% (v/v) NP-40, 1 mM DTT, and protease inhibitor) and placed on ice for 15 min. Lysates were clarified by centrifugation at $21,000 \times g$ for 10 min. The cleared lysate was incubated with NHS beads pre-conjugated with anti-GFP nanobodies for 30 min. The beads were then washed three times by centrifugation using wash buffer (20 mM Tris-HCl (pH 7.5), 150 mM NaCl, 5 mM MgCl₂,1 mM DTT). Washed beads were resuspended in 200 μL of buffer and boiled at 95 °C for 6 min, followed by centrifugation at $21,000 \times g$ for 10 min. The supernatant, with nucleotides, was filtered through pre-washed PVDF centrifugal filters (0.22 μm). Flow throughs were taken for ion-paired reverse phase (IP-RP) HPLC analyses, conducted using an Agilent 1100 Series HPLC and C18 column (Eclipse XDB-C18 5 μm, 4.6 × 150 mm (Agilent)). The running phase was prepared in 500 ml: 6.29 g KH₂PO₄, 1.49 g tetrabutylammonium bromide, and 6.8% (v/v) acetonitrile in water. Each sample was run in the mobile phase at a flow rate of 0.95 ml/min for 9 min at 25 °C with absorbance detected at 252 and 254 nm.

NMR spectroscopy

NMR data were recorded at 298 K or 310 K (In-Cell experiments and controls) on a 600 MHz Bruker Avance III HD spectrometer equipped with QCIP 5 mm cryoprobe or a 800 MHz Bruker Avance III HD spectrometer equipped with triple resonance cryoprobe (nanodisc experiments; QANUC, McGill University). All experiments were recorded using TopSpin (version 3.6.2). NMR samples were prepared in buffer containing 20 mM Tris-HCl (pH 7.5), 100 mM NaCl, 5 mM MgCl₂, 2 mM DTT and 10% D₂O. Two-dimensional ¹H-¹⁵N heteronuclear single quantum coherence (HSQC) (hsqcph) spectra[55] and ¹H-¹⁵N BEST-HSQC (b_hsqcetf3gpsi)[56] were collected to analyze chemical-shift perturbations. Spectra were processed with NMRPipe[57] (version 8.7) and analyzed using NMRView[58] (version 9.2.0). For nanodisc analysis, two-dimensional ¹H-¹³C heteronuclear single quantum coherence (HSQC) (hsqcetgpsp) were used. Nucleotide exchange and hydrolysis assays were conducted by collecting sequential HSQCs to study kinetics. Intrinsic exchange and GEF assays were performed by adding GTPγS at a 10- or 20-fold molar excess (GTPγS:total protein) and SOS^cat was added at molar ratios described in results. To calculate the GDP-bound ratio $[I_{GDP}/(I_{GDP} + I_{GTP})]$, peak intensities were extracted from each individual spectrum using NMRView (version 9.2.0). Exchange curves were plotted and fitted to a single-phase exponential decay function using GraphPad. For intrinsic GTP hydrolysis, peak intensities were extracted and data fit to a one phase exponential association function. For ³¹P NMR measurements, proteins were used at 1 mM concentration in 20 mM Tris-HCl (pH 7.5), 100 mM NaCl, 30 mM MgCl₂, 2 mM DTT and 10% D₂O using a one-dimensional ³¹P standard pulse program (zgig). For the RBD mixing experiment, 5-fold or 2-fold molar excess of RBD was used. *In-Cell NMR experiments:* To prepare IC-NMR samples, 120-300 μM of labeled protein was electroporated into 60×10^6 HEK 293T cells (under passage 25) using a Gene Pulser Xcell Electroporation system (Bio-Rad). For electroporation, cells were resuspended in Opti-MEM and electroporation buffer (200 mM sodium phosphate (pH 7.5), 15 mM HEPES (pH 7.5), 15 mM MgCl₂, 5 mM KCl, 2 mM ATP and 2 mM glutathione). Electroporated cells were immediately transferred into 15 cm dishes for a 5-hour recovery in DMEM supplemented with 20% FBS, penicillin (100 U/mL) and streptomycin (100 μg/mL). Cells were then harvested, washed with PBS, resuspended in a mixture of 250 μL DMEM supplemented with 20% FBS, penicillin and streptomycin and 50 μL of D₂O and were then transferred to a 5 mm NMR tube. IC-NMR experiments were performed at 310 K. A ¹H-¹³C band-selective optimized flip angle short transient heteronuclear multiple quantum coherence (SOFAST-HMQC) (sf_mehmqcgpph) pulse program was used to acquire pure protein reference spectra (9 minutes of acquisition time) and IC-NMR spectra (20 mins−1 h). Spectra were processed with NMRFx Analyst (version 11.4.0) and analyzed using NMRView

(version 9.2.0). Typically, NMR experiments were run with the following parameters: ^{1}H-^{15}N BEST-HSQC for exchange assays used 16 scans, 128 increments (11 min 27 sec acquisition time); 1D ^{31}P NMR used 8 scans, 128 increments (60 min); ^{1}H-^{13}C SOFAST-HMQC on purified proteins in buffer using 16 scans, 128 increments (9 min 40 sec) or with 100 scans, 128 increments (60 min) for runs with RBD, or for In-Cell runs with 150 scans, 90 increments (60 min).

Cell imaging

For immunostaining of electroporated cells: cells were seeded on coverslips precoated with gelatin in 6 well dish and incubated at 37 ˚C in 5% CO2 for 16 h after electroporation in the presence of recombinantly purified FLAG-tagged MRAS fusion proteins. For stable cell lines expressing doxycycline-inducible BirA*/FLAG-tagged MRAS fusion proteins were seeded on coverslips in 6 well dishes and incubated at 37 ˚C in 5% CO2 for 24 h. Cells were induced with 1 μg/ml doxycycline (BioShop) in complete media for 48 h. For immunostaining, cells were washed with PBS and fixed with 4% paraformaldehyde (VWR) 48 h post-transfection. Permeabilization of cells was with PBS containing 0.05% or 0.1% Tween-20 (PBS-T) and blocking with 4% FBS or 2% BSA in PBS-T. Primary antibodies were diluted in blocking reagent and incubated with coverslips for 1 h at 37 ˚C in a humidified chamber. Coverslips were washed with PBS-T and incubated with secondary antibody for 1 hr at 37 ˚C in a humidified chamber (goat anti-rabbit IgG (H + L), Alexa-Fluor 647 (Life Technologies A21244) or goat anti-rabbit IgG (H + L), Alexa-Fluor 555 (Life Technologies A21428), Hoechst (1:2000). Following a final wash with PBS-T and ethanol, coverslips were mounted on slides with the Prolong Diamond antifade mountant (Life Technologies) or with Mowiol (Sigma 81381) and dried for 24 h before acquisition. Imaging of cells was performed using a laser scanning LSM-880 microscope (Zeiss). All images were taken with a 63x objective. 7 to 15 z-stacks were acquired (0.25 μm thickness) for each image and were merged by an XY orthogonal projection with the Zen lite 2.3 software (Zeiss) or Fiji ImageJ software (version 2.3.0). The following laser and detection wavelength were used: Hoechst (excitation 405 nm - detection 455/45 nm), Alexa Fluor 647 (excitation 650 nm−detection 670 nm), Alexa Fluor 555 (excitation 553 nm−detection 568 nm).

Cell culture

Human embryonic kidney epithelial (HEK 293T; ATCC CRL-3216), human cervix epithelial (HeLa; ATCC CCL-2), and human osteosarcoma (U2OS; ATCC HTB-96) cells were maintained in Dulbecco's Modified Eagle's Medium containing 10% fetal bovine serum. For recombinant protein expression, cells were transiently transfected with PEI[59]. Stable cell lines for BioID were generated by lentiviral expression followed by antibiotic selection. For studying MAPK activity, cells were seeded in a 6-well dish in DMEM plus 10% FBS to achieve 50% confluency the next day. Cells were transfected with mutationally activated, Venus-tagged RRAS family GTPases or KRAS, either alone or together with FLAG-tagged ARAF. Cells were then serum starved for 24 h in DMEM alone. As a control, EGF stimulation was carried out by replacing media in the 6-well dish with DMEM containing 50 ng/ml EGF (Gibco, PHG0311L) for 5 mins. Cells were washed with PBS and lysed in RIPA buffer (20 mM Tris-HCl (pH 7.5), 1 mM EDTA, 1% NP40, 0.5% sodium deoxycholate, 0.1% SDS, 140 mM NaCl, 2 mM DTT, 1x Sigma protease inhibitors (P8340), 1 mM PMSF, 5 nM okadaic acid and 1 mM sodium orthovanadate). Equal amounts of cleared lysate were resolved by SDS-PAGE, transferred to nitrocellulose and Western blotted for phospo-ERK1/2, then re-probed for total ERK1/2.

Statistics and reproducibility

Statistical methods used to determine significance are described in the Figure Legends and were calculated using Microsoft Office and GraphPad Prism. All presented Western blots, Coomassie stained gels and microscopy images are representative of at least 3 independent experiments.

Reporting summary

Further information on research design is available in the Nature Portfolio Reporting Summary linked to this article.

Data availability

The mass spectrometry data for MRAS BioID has been deposited to the ProteomeXchange Consortium via the PRIDE archive with the dataset identifier PXD055944. The mass spectrometry data for in-gel digests have the identifier PXD055948. Previously published structures used this work are 5P21 (HRAS-GMPPNP), 4Q21 (HRAS-GDP), 1X1S (MRAS-GMPPNP), and 1X1R (MRAS-GDP). Requests for materials or correspondence should be sent to Matthew Smith (matthew.james.smith@umontreal.ca). Source Data are provided as a Source Data file. Source data are provided with this paper.

References

1. Prior, I. A., Hood, F. E. & Hartley, J. L. The frequency of ras mutations in cancer. *Cancer Res.* **80**, 2669–2974 (2020).
2. Colicelli, J. Human RAS superfamily proteins and related GTPases. *Sci. STKE* **2004**, RE13 (2004).
3. Goh, L. L. & Manser, E. The GTPase-deficient Rnd proteins are stabilized by their effectors. *J. Biol. Chem.* **287**, 31311–31320 (2012).
4. Fueller, F. & Kubatzky, K. F. The small GTPase RhoH is an atypical regulator of haematopoietic cells. *Cell Commun. Signal.* **6**, 6 (2008).
5. Ji, W. & Rivero, F. Atypical Rho GTPases of the RhoBTB subfamily: Roles in vesicle trafficking and tumorigenesis. *Cells* **5**, 28 (2016).
6. Berthold, J., Schenková, K. & Rivero, F. Rho GTPases of the RhoBTB subfamily and tumorigenesis. *Acta Pharmacol. Sin.* **29**, 285–295 (2008).
7. Stiegler, A. L. & Boggon, T. J. The pseudoGTPase group of pseudoenzymes. *FEBS J.* **287**, 4232–4245 (2020).
8. Sasson, Y., Navon-Perry, L., Huppert, D. & Hirsch, J. A. RGK family G-domain:GTP analog complex structures and nucleotide-binding properties. *J. Mol. Biol.* **413**, 372–389 (2011).
9. Chang, D. D. & Colecraft, H. M. Rad and Rem are non-canonical G-proteins with respect to the regulatory role of guanine nucleotide binding in Ca(V)1.2 channel regulation. *J. Physiol.* **593**, 5075–5090 (2015).
10. Quirion, L. et al. Mapping the global interactome of the ARF family reveals spatial organization in cellular signaling pathways. *J. Cell Sci.* **137**, jcs262140 (2024).
11. Rodriguez-Viciana, P., Oses-Prieto, J., Burlingame, A., Fried, M. & McCormick, F. A phosphatase holoenzyme comprised of Shoc2/Sur8 and the catalytic subunit of PP1 functions as an M-Ras effector to modulate Raf activity. *Mol. Cell* **22**, 217–230 (2006).
12. Young, L. C. et al. SHOC2-MRAS-PP1 complex positively regulates RAF activity and contributes to Noonan syndrome pathogenesis. *Proc. Natl. Acad. Sci. USA* **115**, E10576–E10585 (2018).
13. Chin, K. et al. Genomic and transcriptional aberrations linked to breast cancer pathophysiologies. *Cancer Cell* **10**, 529–541 (2006).
14. Hess, K. R. et al. Pharmacogenomic predictor of sensitivity to pre-operative chemotherapy with paclitaxel and fluorouracil, doxorubicin, and cyclophosphamide in breast cancer. *J. Clin. Oncol.* **24**, 4236–4244 (2006).
15. Van De Vijver, M. J. et al. A gene-expression signature as a predictor of survival in breast cancer. *N. Engl. J. Med.* **347**, 1999–2009 (2002).
16. Yasumoto, M. et al. Muscle RAS oncogene homolog (MRAS) recurrent mutation in Borrmann type IV gastric cancer. *Cancer Med.* **6**, 235–244 (2017).

17. Higgins, E. M. et al. Elucidation of MRAS-mediated Noonan syndrome with cardiac hypertrophy. *JCI Insight* **2**, e91225 (2017).

18. Motta, M. et al. Activating MRAS mutations cause Noonan syndrome associated with hypertrophic cardiomyopathy. *Hum. Mol. Genet.* **29**, 1772–1783 (2020).

19. Pires, L. V. L. et al. Atypical, severe hypertrophic cardiomyopathy in a newborn presenting Noonan syndrome harboring a recurrent heterozygous *MRAS* variant. *Am. J. Med. Genet. A.* **185**, 3099–3103 (2021).

20. Suzuki, H. et al. Severe Noonan syndrome phenotype associated with a germline Q71R MRAS variant: a recurrent substitution in RAS homologs in various cancers. *Am. J. Med. Genet. A.* **179**, 1628–1630 (2019).

21. Hauseman, Z. J. et al. Structure of the MRAS–SHOC2–PP1C phosphatase complex. *Nature* **609**, 416–423 (2022).

22. Kwon, J. J. et al. Structure–function analysis of the SHOC2–MRAS–PP1C holophosphatase complex. *Nature* **609**, 408–415 (2022).

23. Liau, N. P. D. et al. Structural basis for SHOC2 modulation of RAS signalling. *Nature* **609**, 400–407 (2022).

24. Bonsor, D. A. et al. Structure of the SHOC2–MRAS–PP1C complex provides insights into RAF activation and Noonan syndrome. *Nat. Struct. Mol. Biol.* **29**, 966–977 (2022).

25. Fernández-Pisonero, I. et al. A hotspot mutation targeting the R-RAS2 GTPase acts as a potent oncogenic driver in a wide spectrum of tumors. *Cell Rep.* **38**, 110522 (2022).

26. Clavaín, L. et al. Characterization of mutant versions of the R-RAS2/TC21 GTPase found in tumors. *Oncogene* **42**, 89–405 (2022).

27. Flex, E. et al. Activating mutations in RRAS underlie a phenotype within the RASopathy spectrum and contribute to leukaemogenesis. *Hum. Mol. Genet.* **23**, 4315–4327 (2014).

28. Traut, T. W. Physiological concentrations of purines and pyrimidines. *Mol. Cell. Biochem.* **140**, 1–22 (1994).

29. Smith, M. J., Neel, B. G. & Ikura, M. NMR-based functional profiling of RASopathies and oncogenic RAS mutations. *Proc. Natl. Acad. Sci. Usa.* **110**, 4574–4579 (2013).

30. Ohba, Y. et al. Regulatory Proteins of R-Ras, TC21/R-Ras2, and M-Ras/R-Ras3 *. *J. Biol. Chem.* **275**, 20020–20026 (2000).

31. Denisov, I. G., Grinkova, Y. V., Lazarides, A. A. & Sligar, S. G. Directed self-assembly of monodisperse phospholipid bilayer nanodiscs with controlled size. *J. Am. Chem. Soc.* **126**, 3477–3487 (2004).

32. Mazhab-Jafari, M. T. et al. Membrane-dependent modulation of the mTOR Activator Rheb: NMR observations of a GTPase tethered to a lipid-bilayer nanodisc. *J. Am. Chem. Soc.* **135**, 3367–3370 (2013).

33. Mazhab-Jafari, M. T. et al. Oncogenic and RASopathy-associated K-RAS mutations relieve membrane-dependent occlusion of the effector-binding site. *Proc. Natl Acad. Sci.* **112**, 6625–6630 (2015).

34. Findlay, G. M. et al. Interaction domains of Sos1/Grb2 are finely tuned for cooperative control of embryonic stem cell fate. *Cell* **152**, 1008–1020 (2013).

35. Grudzien, P., Jang, H., Leschinsky, N., Nussinov, R. & Gaponenko, V. Conformational dynamics allows sampling of an "Active-like" state by oncogenic K-Ras-GDP. *J. Mol. Biol.* **434**, 167695 (2022).

36. Spoerner, M. et al. Conformational states of human rat sarcoma (Ras) protein complexed with its natural ligand GTP and their role for effector interaction and GTP hydrolysis. *J. Biol. Chem.* **285**, 39768–39778 (2010).

37. Long, D. et al. A Comparative CEST NMR study of slow conformational dynamics of Small GTPases complexed with GTP and GTP analogues. *Angew. Chem. Int. Ed.* **52**, 10771–10774 (2013).

38. Sharma, A. K. et al. Revealing the mechanism of action of a first-in-class covalent inhibitor of KRASG12C (ON) and other functional properties of oncogenic KRAS by 31P NMR. *J. Biol. Chem.* **300**, 105650 (2024).

39. Watanabe-Takano, H., Takano, K., Keduka, E. & Endo, T. M-Ras is activated by bone morphogenetic protein-2 and participates in osteoblastic determination, differentiation, and transdifferentiation. *Exp. Cell Res.* **316**, 477–490 (2010).

40. Adhikari, H. & Counter, C. M. Interrogating the protein interactomes of RAS isoforms identifies PIP5K1A as a KRAS-specific vulnerability. *Nat. Commun.* **9**, 3646 (2018).

41. Araki, M., Yoshimoto, K., Ohta, M., Katada, T. & Kontani, K. Development of a versatile HPLC-based method to evaluate the activation status of small GTPases. *J. Biol. Chem.* **297**, 101428 (2021).

42. Smith, M. J. & Ikura, M. Integrated RAS signaling defined by parallel NMR detection of effectors and regulators. *Nat. Chem. Biol.* **10**, 223–230 (2014).

43. Zhao, Q. et al. Real-time in-cell NMR reveals the intracellular modulation of GTP-bound levels of RAS. *Cell Rep.* **32**, 108074–108074 (2020).

44. Ye, M. et al. Crystal structure of M-Ras reveals a GTP-bound 'off' state conformation of Ras family small GTPases. *J. Biol. Chem.* **280**, 31267–31275 (2005).

45. Sulahian, R. et al. Synthetic Lethal Interaction of SHOC2 Depletion with MEK Inhibition in RAS-driven cancers. *Cell Rep.* **29**, 118–134.e8 (2019).

46. Samavarchi-Tehrani, P., Abdouni, H., Samson, R. & Gingras, A.-C. A versatile lentiviral delivery toolkit for proximity-dependent biotinylation in diverse cell types. *Mol. Cell. Proteom.* **17**, 2256–2269 (2018).

47. Roux, K. J., Kim, D. I., Raida, M. & Burke, B. A promiscuous biotin ligase fusion protein identifies proximal and interacting proteins in mammalian cells. *J. Cell Biol.* **196**, 801–810 (2012).

48. Couzens, A. L. et al. Protein interaction network of the Mammalian Hippo pathway reveals mechanisms of kinase-phosphatase interactions. *Sci. Signal.* **6**, rs15 (2013).

49. Liu, G. et al. ProHits: integrated software for mass spectrometry–based interaction proteomics. *Nat. Biotechnol.* **28**, 1015–1017 (2010).

50. Kessner, D., Chambers, M., Burke, R., Agus, D. & Mallick, P. ProteoWizard: open source software for rapid proteomics tools development. *Bioinformatics* **24**, 2534–2536 (2008).

51. Pedrioli, P. G. A. Trans-proteomic pipeline: A pipeline for proteomic analysis. in *Proteome Bioinformatics* (eds. Hubbard, S. J. & Jones, A. R.) vol. 604 (Humana Press, Totowa, NJ, 2010).

52. Shteynberg, D. et al. iProphet: Multi-level integrative analysis of shotgun proteomic data improves peptide and protein identification rates and error estimates. *Mol. Cell. Proteom.* **10**, M111.007690 (2011).

53. Teo, G. et al. SAINTexpress: Improvements and additional features in significance analysis of INTeractome software. *J. Proteom.* **100**, 37–43 (2014).

54. Schellenberg, M. J., Petrovich, R. M., Malone, C. C. & Williams, R. S. Selectable high-yield recombinant protein production in human cells using a GFP/YFP nanobody affinity support. *Protein Sci.* **27**, 1083–1092 (2018).

55. Bodenhausen, G. & Ruben, D. J. Natural abundance nitrogen-15 NMR by enhanced heteronuclear spectroscopy. *Chem. Phys. Lett.* **69**, 185–189 (1980).

56. Lescop, E., Schanda, P. & Brutscher, B. A set of BEST triple-resonance experiments for time-optimized protein resonance assignment. *J. Magn. Reson* **187**, 163–169 (2007).

57. Delaglio, F. et al. NMRPipe: A multidimensional spectral processing system based on UNIX pipes. *J. Biomol. NMR* **6**, 277–293 (1995).

58. Johnson, B. A. Using NMRView to Visualize and Analyze the NMR Spectra of Macromolecules. in *Protein NMR Techniques* (ed. Downing, K.) (Humana Press, Totowa, N.J., 2004).

59. Werth, S. et al. A low molecular weight fraction of polyethylenimine (PEI) displays increased transfection efficiency of DNA and siRNA in fresh or lyophilized complexes. *J. Controlled Release* **112**, 257–270 (2006).

Author contributions

M.J.S. conceived and designed the project. G.B.A., R.S., C.H.J., E.T. and R.C.K. performed experiments and analyzed data. The manuscript was prepared by G.B.A. and M.J.S. with input from R.S. and C.H.J.

Competing interests

The authors declare no competing interests.

Additional information

Supplementary information The online version contains supplementary material available at https://doi.org/10.1038/s41467-025-55967-y.

Correspondence and requests for materials should be addressed to Matthew J. Smith.

Peer review information *Nature Communications* thanks Hema Adhikari, Noritaka Nishida and the other, anonymous, reviewer for their contribution to the peer review of this work. A peer review file is available.

Reprints and permissions information is available at http://www.nature.com/reprints

Publisher's note Springer Nature remains neutral with regard to jurisdictional claims in published maps and institutional affiliations.